Cement and Concrete Composites 148 (2024) 105469

Contents lists available at ScienceDirect

Cement and Concrete Composites

journal homepage: www.elsevier.com/locate/cemconcomp

Fresh, mechanical, and microstructural properties of lithium slag concretes

SM Arifur Rahman, Faiz Uddin Ahmed Shaikh *, Prabir Kumar Sarker

Civil Engineering Discipline, School of Civil and Mechanical Engineering, Curtin University, Perth, Australia

ARTICLE INFO

Keywords:
Lithium slag
Fly ash
Green concrete
Cenosphere
Fresh properties
Mechanical properties
Interfacial transition zone
Microstructure

ABSTRACT

Lithium slag (LS) is a by-product of the lithium salt purification process, and this can be used as a partial replacement of cement for the production of green concrete by reducing carbon footprint associated with clinker production. The raw-LS is rich in aluminosilicate, containing 77.2 % of SiO_2+Al_2O_3+Fe_2O_3, 31.6 % of amorphous phases, and the loss of ignition is 7.8 % at 750 °C, making it a suitable pozzolan by providing 4.8 times higher ion dissolution capacity at 1 day compared to class F fly ash (FA). In this study, fresh properties, mechanical, and microstructural properties of 0–60 % cement replaced LS concretes were thoroughly determined with a total binder content of 400 kg/m^3 and water-binder ratio of 0.435, and the properties were compared with the same mix proportion of FA concrete. The results show that 20–60 % LS concrete mixes produced normal density concrete within the design slump of 125 ± 25 mm and air content of 2 ± 0.5 %. At 90 days, the average compressive strength, tensile strength, and elastic modulus of 40 % LS concrete were 58.6 MPa, 4.10 MPa, and 39 GPa, respectively, which are higher compared to 40 % FA concrete of 35.5 MPa, 3.0 MPa, and 31.1 GPa, respectively, revealing that LS concrete offers better mechanical strength. However, mechanical strengths decreased significantly beyond 40 % LS incorporation. The experimentally determined 28 days mechanical strengths of 40 % LS concrete were underestimated by ACI 318 and AS 3600 standard equations. The BSE-EDS on the ITZ of fine and coarse aggregate confirmed a consistent development of amorphous and amorphous intermediate hydration products in the development of mechanical properties of LS concrete mixes.

1. Introduction

The pursuit of sustainable construction practices is an imperative response to the challenges posed by the growing environmental concerns associated with traditional construction materials and techniques. Within this context, supplementary cementitious materials (SCMs) have emerged as a key strategy to mitigate the carbon footprint of the concrete while enhancing the workability, mechanical performance, and durability of concrete. Lithium slag (LS) is a by-product of the lithium salt purification process. It is emerging as a potential SCM to produce green concrete [1,2]. This research is motivated by the potential pozzolanic activity of LS by using high-volume LS as a SCM in the production of sustainable concrete, and assessing the fresh state, mechanical, and microstructural properties.

The utilization of pozzolanic materials like lithium slag (LS) in concrete production is an emerging trend in sustainable construction. These materials react with calcium hydroxide generated during cement hydration, forming additional calcium silicate hydrate (C–S–H) gel to impart strength and durability of concrete by producing more amorphous and amorphous intermediate hydration products [3]. Despite its status as a hazardous material, containing heavy metals, and often consigned to landfills, LS presents a unique opportunity for transformation [1,4,5]. In particular, aluminosilicate-rich raw LS is a competitive candidate as a new pozzolan since the sum of SiO_2, Al_2O_3, and Fe_2O_3 content is 77.2 %, and amorphousness is 31.6 % [6]. The 7.8 % loss of ignition (LOI) at 750 °C further underscores its pozzolanic potential [6]. Researchers assessed the pozzolanic activity of LS through different tests. Specifically, LS provided 889 mg/g pozzolanic activity at 28 days and reduced 50 % initial electrical conductivity within 7 days in 1 g/L unsaturated lime solution [6]. This acceleration in pozzolanic activity holds a significant promise for enhancing the sustainability of concrete production. Recent studies have demonstrated that 30 % LS in concrete has resulted in compressive strengths as high as 52 MPa [7] and 44 MPa [8], while the strength activity indices (SAIs) were 86 % [7] and 110 % [8] at 28 days.

Moreover, the application of LS in mortar has produced equally notable results, achieving compressive strengths of 55 MPa [9] and 52 MPa [10] at 28 days and the SAIs of 97 % [9] and 96 % [10]. When used

* Corresponding author.
E-mail address: S.Ahmed@curtin.edu.au (F.U.A. Shaikh).

https://doi.org/10.1016/j.cemconcomp.2024.105469
Received 11 November 2023; Received in revised form 21 January 2024; Accepted 1 February 2024
Available online 2 February 2024

at a higher cement replacement level of 40 %, LS has shown to contribute 48 MPa [6] and 42 MPa [11] of compressive strength in paste and mortar specimens at 28 days. Researchers also determined the tensile strength, flexural strength, and elastic modulus for 25 % LS in the production of concrete with 0–100 % recycled coarse aggregate, and these properties were predicted by the Chinese standard GB50010 [12,13].

In comparison, class F fly ash (FA) has been widely benchmarked against various novel natural and artificial pozzolans for partial cement replacement [14–18]. FA is known for its pozzolanic activity, which can reach up to 780 mg/g pozzolanic activity at 28 days [19]. The increase in the pozzolanic activity proportionally enhances the early and long-term mechanical strength and microstructure development. Its application at 50 % cement replacement has resulted 34 MPa and 65 MPa of compressive strength at 28 and 180 days, while imparted SAIs of 67 % and 101 %, respectively [20]. Furthermore, FA as a SCM reduces water demand in concrete [21], as its spherical shaped particle morphology provide ball bearing effect in the mixture [22], whereas LS particles are flaky and irregular, needs in-depth study to understand the fresh properties of high volume LS concrete. Researchers found that 50 % FA as a SCM could reduce 40 % CO_2 emissions [20,23,24]. This is a part of the effort to make cement production more sustainable by substituting clinker with natural pozzolans without compromising the cement properties. Therefore, this study finds the opportunity to use high-volume LS (up to 60 %) as a sustainable alternative to FA, and compare LS performance with FA concrete to examine their correlations with standard equations [25–27].

Australia's construction industry is facing a challenge due to the impending scarcity of FA, a common SCM, due to the closure of coal-based power plants [28]. While this closure will help reduce carbon emissions, it will inadvertently affect the supply of FA, which is crucial for sustainable concrete production. As a result, there is a pressing need to explore local and sustainable pozzolanic materials like LS as an alternative. Therefore, using LS as a SCM in the production of concrete is not only an environmental necessity but most importantly, a strategic response to the changing dynamics of construction materials in Australia [11].

This research presents a thorough analysis of the fresh properties, mechanical characteristics, and microstructural attributes of high-volume LS concrete. By comparing 0–60 % cement replaced LS concrete to traditional FA-based mixes, this study contributes significantly to sustainable construction practices. It provides valuable insights for engineers, researchers, and industry stakeholders navigating the evolving landscape of construction materials and techniques in Australia. The significance of this research rests not only in its potential to unlock the pozzolanic activity of LS but also in addressing pressing questions surrounding the environmental impact of construction, the need for local and sustainable pozzolanic materials, and the prospects of mitigating the scarcity of FA. In a world coping with the sustainability challenges, LS emerges as a promising SCM, and it aligns well with the search for greener concrete ingredients.

2. Materials and methods

2.1. Materials

In this study, cement, LS, and FA (class F) were used as the binders and their grain size distribution is shown in Fig. 1. Commercially manufactured ordinary Portland cement satisfied the standard requirements [29]. The water consistency [30] of cement was 30 %, soundness [31] of 0 mm, and the initial and final setting times [32] were 133 and 210 min, respectively [11]. The LS and FA were sourced from Western Australia and their CaO contents were 7.5 and 4.3 %, respectively. The major oxides composition in mass percentage, LOI, amorphousness, specific gravity, median particle size (d_{50}), specific surface area, electrical conductivity (EC) and pH of cement [6], LS [6], and FA [33,34] are shown

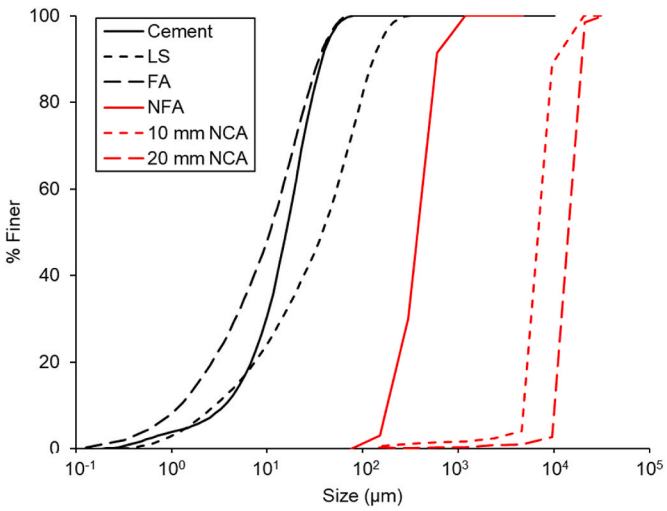

Fig. 1. Grain size distribution of cement [6], lithium slag (LS) [6], class F fly ash (FA) [33,34], natural fine aggregate (NFA) [11], 10 mm natural coarse aggregate (NCA), and 20 mm NCA.

in Table 1. Here, 1 g of the binder was added in 70 mL of deionised (DI) water and kept at 25 °C to determine EC and pH after 24 h.

The reactivity of the pozzolans were further characterised from the electrical conductivity (EC) test for 90 days and the detailed method of the EC measurement was followed from the previous published research [6]. Fig. 2 presents the change in EC and relative conductivity (RC) of LS and FA in 1 g/L lime water and DI water with time, respectively. The RC is the ratio of the difference between initial and instantaneous conductivity to the initial conductivity of a system [3]. It can be seen that the EC increased in DI water for LS and FA, while the EC rapidly decreased in the unsaturated lime water, which represents a pozzolanic reactivity of the SCMs. Specifically, the rapid decrease of EC for LS in unsaturated lime water was caused by early ion dissolution of LS soluble salts and the reaction equilibrium was settled at 1100 h. Nonetheless, a slow ion dissolution of FA in unsaturated lime water extended the reaction equilibrium by 288 h compared to LS system. Fig. 2 also represents the variation in the RC of the SCMs with time. Here, the RC of LS proportionally increases with time, while FA showed an abnormal variation of RC from the reaction initiation. Particularly, LS reduced 14 % EC at 100 s, and in contrast, FA elapsed 10^6 s to attain same RC. Therefore, the initial activation potential of FA was roughly lagged by 11.6 days (10^6 s) compared to LS to gain same initial reactivity at 100 s. Additionally, the RC of LS and FA was compared with the findings of Payá et al. [35], as

Table 1
The major oxides composition in mass percentage, LOI, specific gravity, d_{50}, SSA, and EC of the cement, LS, and FA.

Parameters		Cement	LS	FA
Oxides composition (%)	SiO_2	20.7	54.6	51.1
	Al_2O_3	5.7	21.1	25.6
	Fe_2O_3	2.9	1.5	12.5
	CaO	63.1	7.5	4.3
	MgO	1.3	0.6	1.5
	SO_3	3.3	5.6	0.2
	K_2O	0.4	0.9	0.7
	Na_2O	0.3	0.7	0.8
LOI at 750 °C (%)		1.90	7.80	0.57
Physical properties	Amorphous content, %	–	31.6	54.6 [33,34]
	Specific gravity	3.10	2.46	2.20
	d_{50}, μm	17	38	10
	Specific surface area, kg/m^2	360	342	416
	EC, μS/cm	3420	1300	270
	pH	12.60	11.28	12.17

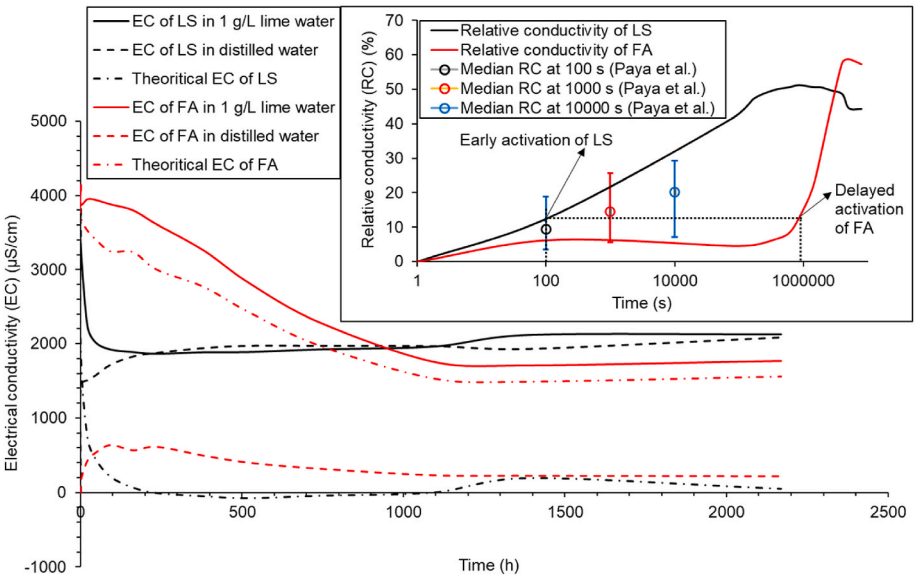

Fig. 2. Electrical conductivity (EC) and relative conductivity (RC) of LS [6] and FA. Here, theoretical EC at an instant is the difference of the EC of pozzolan in 1 g/L lime water and the EC of pozzolan in distilled water.

shown in Fig. 2. The maximum, minimum, and median values of the RC of 10 different FA were scatter plotted at 10^2, 10^3, and 10^4 s, and the RC of LS and FA were roughly within the significant RC range of low calcium FA. Therefore, the variation of the EC and RC over time will certainly provide the justification in the development of early and long-term mechanical properties of LS and FA concrete products.

The BSE coupled layered EDS elemental colour mapping images of cement, LS, and FA are shown in Fig. 3. The cement grains are irregular shaped, and it predominantly contains Ca, Al, and Si elements, as shown in Fig. 3 (a). The LS grains are also irregular, contains cenosphere, and rod shaped sulphur rich particles, and the major elemental composition contains Si, Al, and Ca, as shown in Fig. 3 (b). The FA particles are mostly round with small number of cenosphere particles, and mostly contain Fe, Ca, Na, K, and Mg elements in different amorphous aluminium-silicate phases [36], as depicted in Fig. 3 (c). The relative composition of cement minerals was 64 % tricalcium silicate, 15.2 % larnite, 9.7 % tricalcium aluminate, 6.6 % brownmillerite, 2.6 % gypsum, and 1.9 % portlandite [6]. Then, LS holds 2.1 % β-spodumene, 6.6 % bassanite, 5.4 % calcium magnesium carbonate, 23.8 % quartz, 28.2 % anorthite, 2.3 % albite, and 31.6 % amorphous phases [6]. Lastly, the phase abundance of FA was 1.6 % hematite, 3.5 % maghemite, 2.3 % magnetite, 16.2 mullite, and 21.8 % quartz, and 54.6 % amorphous phase [33,34].

In this study, natural quarry sand as natural fine aggregate (NFA) containing 98 % crystalline silica was used [11]. Natural crushed granite of 20 mm and 10 mm nominal size natural coarse aggregates (NCA) were used. The particle size distribution of the NFA, 10 mm and 20 mm NCA is shown in Fig. 1. The water absorption capacity of the NFA, 10 mm, and 20 mm NCA was 0.43, 0.37, and 0.65 %, respectively, and the specific gravity was 2.61, 2.67, and 2.74, respectively. The median grain size of the NFA, 10 mm, and 20 mm NCA was 380 µm, 7.1 mm, and 10.6 mm, respectively. The workability of the concrete mixture was enhanced by a commercial organic superplasticizer (SP) [37]. The density, solid content, and viscosity of the SP were 1.1 g/cm^3, 40 %, and 145 mPas (23 °C), respectively. The drinking quality water was used for the concrete mix as specified in AS 1379 [38], and the total dissolved solids of the water was 195 ± 65 ppm.

2.2. Mix proportions

The mix proportions of the concrete ingredients are shown in Table 2. Primarily, the control mix was designed for 40 MPa compressive strength at 28 days, 125 ± 25 mm of slump, and 2 ± 0.5 % air content. The cement content, aggregate-binder ratio, and water-binder ratio (w/b) of the control mix as a normal strength concrete were 400 kg/m^3, 4.25, and 0.435, respectively. The cement content of LS concretes and FA concretes was partially replaced by 20–60 % LS and 20–60 % FA, respectively. The SP content of 40 and 60 % LS concrete mixes was determined from the trail mixes, and the workability of the fresh mixes were adjusted by adding 1.5 wt% and 2 wt% of the binder. The appropriate amount of SP was mixed into water and stirred for complete dispersion. The aggregates were washed to remove fines and visible contaminants, followed by drying at ambient temperature until the aggregates met saturated surface dry (SSD) condition [38]. The SSD conditioned NFA and NCA were placed into a clean 70 L pan mixture confirming AS 1379 [38] specifications, and the mixture was rotated for 2 min. Later, binder was added into the mixture, and the dry mix was continued for again 2 min, followed by the addition of water with/-without SP within the time interval. Then, the mix was scrapped from the sides of the mixer to the centre within 60 s, and the mix was further homogenized by applying 2 min mixing. The fresh concrete mix was then tested for the fresh properties, and finally placed in appropriate moulds in two layers by using a vibrating table as specified in AS 1012.5 [39]. The moulded fresh concrete was ambient cured for 24 h at 22 ± 2 °C temperature with 65 ± 5 % relative humidity. Finally, the concrete specimens were demoulded and cured in 2 g/l lime water tank at 22 ± 2 °C temperature. The control concrete and LS and FA concretes were tested at specified ages.

2.3. Methodology

2.3.1. Fresh properties

The freshly prepared LS and FA concretes were parallelly tested for slump, air content, fresh density, water retention capacity (WRC), and compaction factor tests. The slump [40] was determined by using a moist and clean standard slump cone, followed by pouring fresh concrete in three layers and blowing each layer with 25 uniform strokes. The slump of the fresh concrete was then determined with a steel tape with respect to the height of the slump cone upon lifting up the slump cone vertically upward, as shown in Fig. 4 (a). Concurrently, the air content of the fresh concrete was determined from the air content meter confirming standard requirements [41], and two consecutive tests were

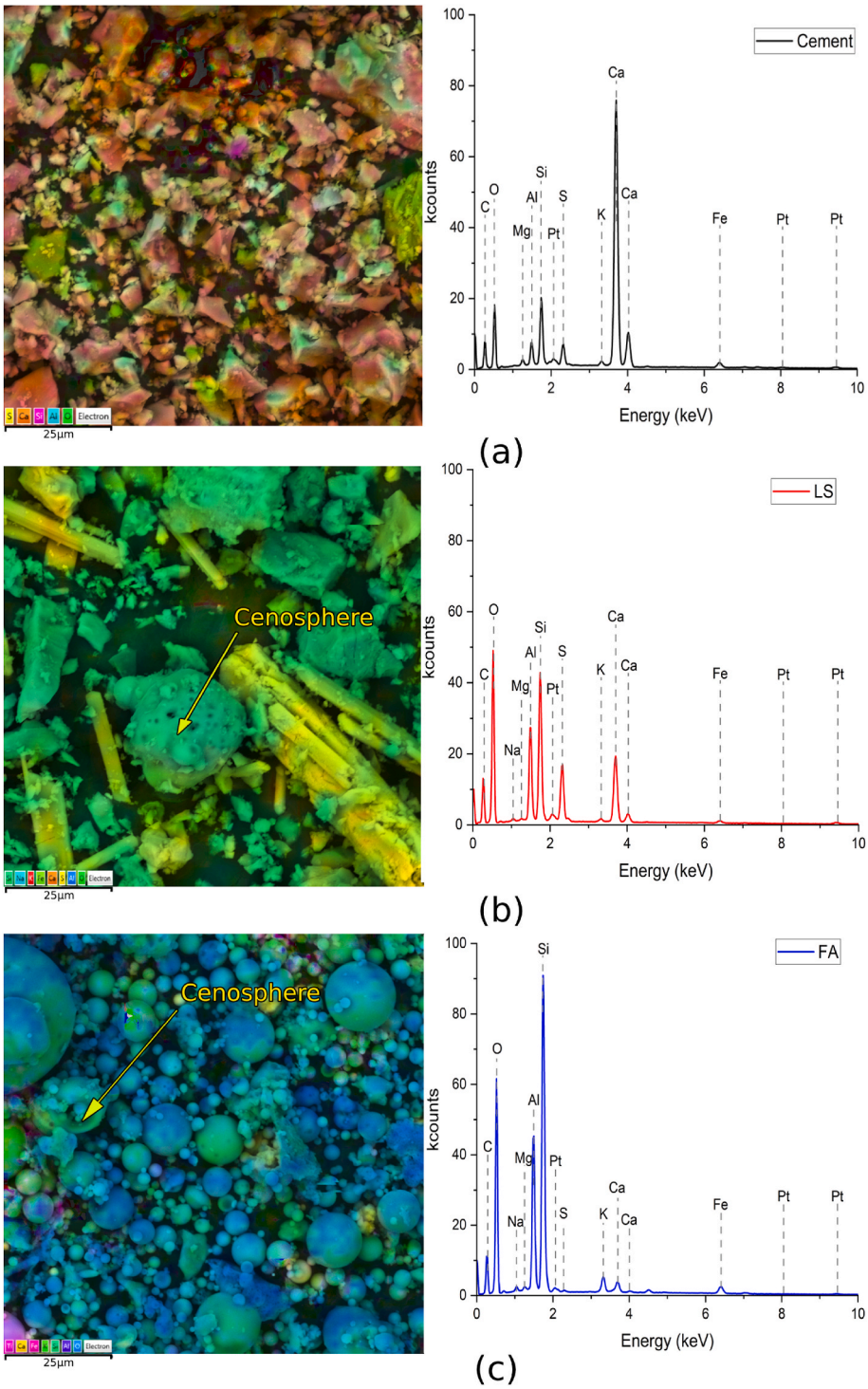

Fig. 3. BSE coupled layered EDS elemental colour mapping and element spectra of cement (a), LS (b), and (c) FA at 20 keV voltage. (For interpretation of the references to colour in this figure legend, the reader is referred to the Web version of this article.)

performed for each batch. The fresh concrete was placed in three layers, and each layer was compacted by 70 strokes, followed by tamping on the side walls by a rubber mallet. The air content of the fresh mix was recorded from the analogue pressure dial gauge by releasing the entrapped air valve for 30 s after the system reaches at airtight condition. The fresh density [39] of the concrete was determined with an air content determination measuring bowl of size 300 mm (height) 320 mm (diameter) complying AS 1012.4.1 [42] requirements. The fresh concrete was compacted as detailed in air content test, and weighed in a balance with an accuracy of 0.1 g. The compaction factor of the fresh concrete was determined from the AS 1012.3.2 [43] specification. The fresh concrete was placed in the moist and cleaned top hopper within 4 min after the concrete mix, and the trapdoor was opened to move the concrete to lower hopper, and then to the base cylinder. The partially compacted concrete cylinder was weighed after removing the excess concrete on the top of the cylinder by a straight edge. Later, the concrete inside the cylinder was emptied, and the cylinder was again filled with fresh concrete, vibrated in two layers, and finally the fully compacted

Table 2
Mix proportions of concrete ingredients.

Mix ID	Binders (kg)			Aggregates (kg)			Water (kg)	SP[a]
	Cement	LS	FA	20 mm NCA	10 mm NCA	NFA		
Control	400	–	–	789	393	679	174	–
20 % LS	320	80	–	789	393	679	174	–
40 % LS	240	160	–	789	393	679	174	1.5
60 % LS	160	240	–	789	393	679	174	2.0
20 % FA	320	–	80	789	393	679	174	–
40 % FA	240	–	160	789	393	679	174	–
60 % FA	160	–	240	789	393	679	174	–

[a] SP quantity in wt.% of binder.

(a)

(b)

Fig. 4. Slump (a) and (b) water retention test of fresh concrete.

fresh concrete was weighed. The compaction factor of the fresh concrete was determined from the mass ratio of the partially compacted to the fully compacted concretes. Finally, the mortar was separated from each batch of freshly prepared concrete mixes and tested for water retention capacity (WRC) [44], as shown in Fig. 4 (b). The WRC of each batch was determined from the ratio of the flow of the mortar after applying 7 ± 0.4 kPa vacuum pressure for 1 min to the mortar flow at normal atmospheric pressure. The fresh tests were completed within 15 min after completing the concrete mixing protocols.

2.3.2. Mechanical properties

The determination of mechanical properties of LS and FA concrete specimens includes compressive strength, split tensile strength, flexural strength, and elastic modulus. The mechanical properties of the concretes are measured at 7, 28 and 90 days. It is essential to assess the long-term strength development of high volume of newly characterised LS as a pozzolan. The compressive strength of all concrete mixes was determined by preparing four 100 × 200 mm cylinders and tested at a loading rate of 0.333 MPa/s in MCC8 universal testing machine (UTM) with 3000 kN compression loading capacity. Later, the split tensile strength of the three 150 × 300 mm concrete cylinders from each mix was determined at a loading rate 0.025 MPa/s in MCC8 UTM. Flexural strengths [45] of three 100 × 100 × 400 mm prismatic concrete specimens was determined using the Shimadzu 300 kN UTM with a loading rate of 0.0166 MPa/s. The lower steel roller supports were 300 mm apart and two top loading rollers were kept at one-third of the span length. Finally, The elastic modulus [46] of three 100 × 200 mm cylindrical specimens was determined by using highly sensitive 2-wire quarter bridge circuit strain gauges of length 30 mm, 120 ± 0.5 Ω resistance, and 2.09 ± 1 % gauge factor. The concrete cylinder top surface was polished by using a concrete grinder. Primarily, the strain gauge position on the concrete surface was cleaned with #120 abrasive paper and the dust was removed by isopropyl alcohol. This sequence was followed till a flat surface was obtained without air bubble. The strain gauge was attached lead wire and fitted on the concrete surface by using manufacturer recommended adhesive. Finally, the lead wire was connected to the data logger ports and the stress versus strain data was decoded in the Matest 3000 kN UTM by applying a three-cycle loading system that uniformly increases from 3 MPa (pre-load) to 40 % of the average compressive strength at a loading rate of 0.25 MPa/s. The development of mechanical strength of the concrete specimen at different ages are expressed with relative to the control specimen's mechanical strength. Therefore, the SAI is the ratio of the compressive strength at a specified age to the compressive strength of the control specimen same age multiplied by 100 %. On the other hand, the relative split tensile strength, flexural strength, and elastic modulus of a concrete specimen were expressed as the ratio of the mechanical strength at a specified age to the mechanical strength of the control specimen same age multiplied by 100 %.

2.3.3. Microstructure investigation

Two 5 × 5 mm size concrete specimens containing two faces of coarse aggregates were cut from the concrete cylinder by a brick saw machine with a nominal thickness of 2~3.5 mm. The specimens were kept at 40 °C for 72 h and ethanol was exchanged after each 24 h to stop the hydration [6]. Later, the specimens were coated with 5 nm carbon coating and analysed in TESCAN MIRA3 FEG-SEM at high vacuum pressure, 20 kV voltage, and beam intensity of 14.0 under BSE detector. Finally, the hydration products were characterised by applying EDS.

3. Results and discussions

3.1. Fresh properties

The variation of the slump [40] of freshly prepared LS and FA concrete mixes are depicted in Fig. 5 (a). The 40 % LS mix showed the average maximum slump of 125 mm, while the minimum slump was 110 mm for the control mix. Overall, the slump of the fresh mixes was within the designed slump range of 125 ± 25 mm. The average slump produced by 20 % LS mix was equal to the control mix, however the average slump was slightly increased by 5 mm for the 20 % FA concrete mix in the same comparison. The slump of both 40 % LS and 60 % LS mixes was 125 mm, which was achieved by adding 1.5 wt% and 2.0 wt% of binder SP. The addition of SP in 40 % LS and 60 % LS mixes is based on two key observations. Firstly, both LS and FA contain cenospheres, as shown in Fig. 3 (b) and 3 (c), respectively. Cenospheres are microparticles with a hollow spheroid structure and range from 1 to 600 μm in

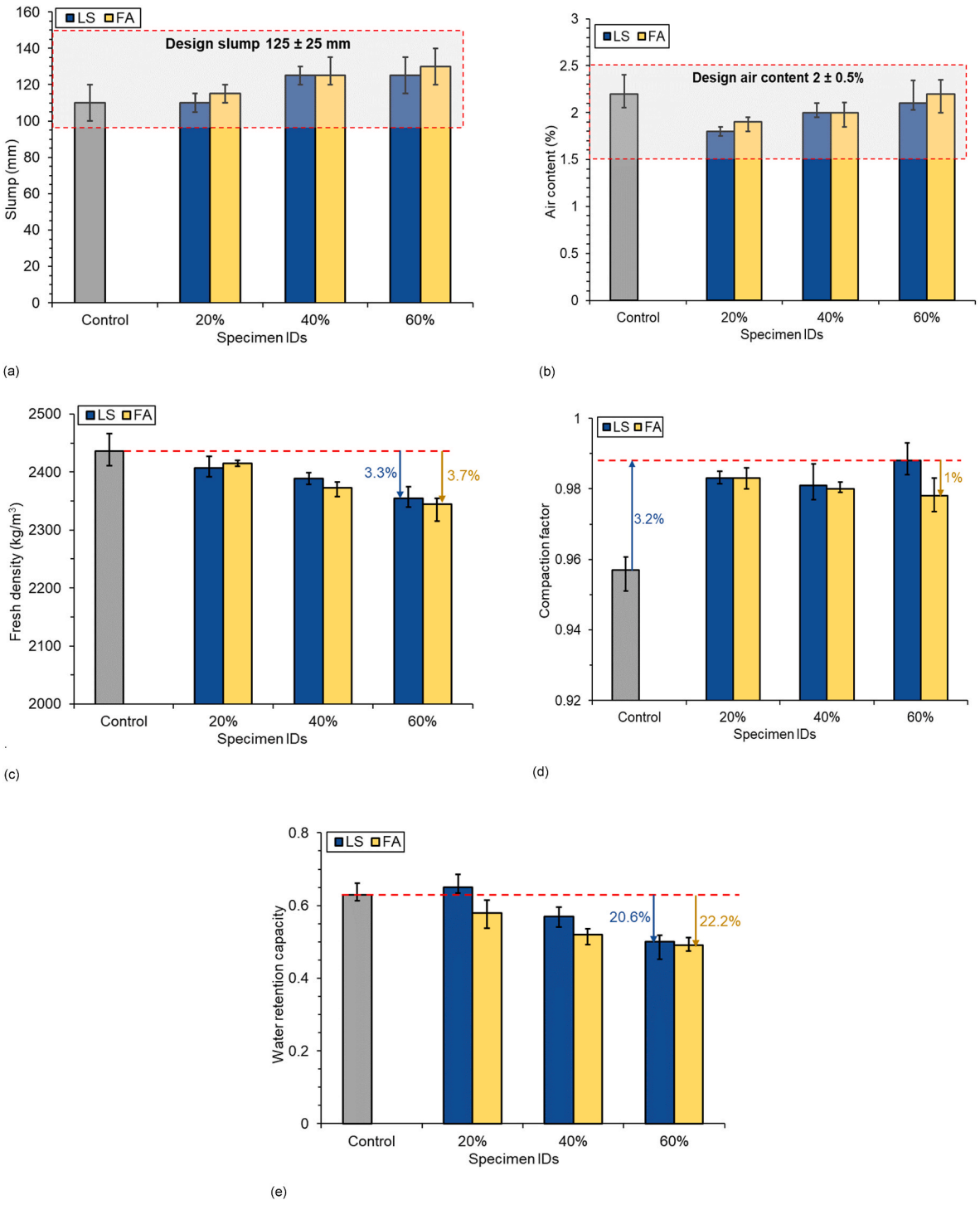

Fig. 5. Variation of slump (a), air content (b), fresh density (c), compaction factor (d), and (e) water retention capacity of control, 20–60 % LS, and 20–60 % FA concrete mixes.

size for FA [47]. Cenospheres lead to higher water absorption and more permeable pores in concrete [48], while typically reducing its density and maintaining mechanical strength [47]. Secondly, the particles in LS are irregular and flaky, contrasting with the smoother, ball-bearing-like nature of FA particles [22,49]. This difference in morphology affects the flowability of the concrete mix. The FA particles facilitate a lubricating effect, enhancing workability, whereas the irregular and flaky nature of LS particles necessitates the use of SP to maintain adequate workability without having harmful materials like chlorides or triethanolamine for early strength development [37]. In conclusion, the higher amount of irregular and flaky LS particles, coupled with the presence of cenospheres, necessitates the use of SP to attain the design slump and air content. Therefore, appropriate SP dosages was used for 40 % LS and 60 % LS mixes to achieve the desired workability despite the higher median particle size and lower specific surface area of LS compared to FA. As a result, the slump of 20–60 % FA concrete mixes was increased by 5–20 mm compared to the control.

The air content [41] of the fresh mixes is shown in Fig. 5 (b). Overall, the air content of the concrete mixes decreased with the increase of the LS as a partial replacement of cement, while an inversely proportional

relationship was found for FA in the same comparison. The air content of the fresh mixes was determined and conforming design air content 2 ± 0.5 %. The initial 0.4 and 0.3 % decrease in the air content for 20 % LS and 20 % FA mix may be due to the cenosphere particles. In contrast, appropriate SP dosage was provided to adjust the workability of 40 % LS and 60 % LS mixes, and the air content of the mixes was increased by 0.2 and 0.3 % compared to the 20 % LS mix. Similarly, the increase in slump of 40 % FA and 60 % FA fresh concrete mixes also supported the surge 0.1 and 0.3 % air content, respectively compared to 20 % FA mix.

The fresh density [39] of the concrete mixes is shown in Fig. 5 (c). The fresh density of the control mix was 2436 kg/m^3. It is seen that the fresh density of concrete decreases with the increase of LS and FA content in the mixes. The fresh density of 20–60 % LS and 20–60 % FA concrete mixes was reduced by 1.2–3.3 % and 0.9–3.7 %, respectively. The fresh density of LS and FA concrete mixes was slightly less than the control mix, but compliant with normal concrete fresh density of 2200–2600 kg/m^3 [50]. Therefore, the reduction of the fresh density of LS and FA concrete mixes was attributed due to the lower specific gravity of LS and FA compared to cement.

The compaction factor [43] of LS and FA concrete mixes is given in Fig. 5 (d). The compaction factor of the control was 0.957. The compaction factor of 20–60 % LS concrete did not follow a particular trend with respect to the LS content as a partial replacement of cement. The compaction factor of 20 % LS, 40 % LS, and 60 % LS mixes was increased by 2.7, 2.5, and 3.2 %, respectively. On the other hand, the 20 % FA as a SCM produced better compacted concrete than the control, however the compactibility degrade for 40–60 % FA as a SCM. Specifically, the compaction factor of 20 % FA, 40 % FA, and 60 % FA mixes was increased by 2.7, 2.4, and 2.2 %, respectively. The variation of the compaction factor of different mixes depends on the leanness and richness of the mix [50]. Fresh concrete mixes with lower fresh density and high slump produce leaner concrete mix, while rich fresh mixes are of high fresh density and low slump. Therefore, lean concrete prepared with 40–60 % LS as a SCM needs 1.5–2 wt% (of binder) SP to reduce the friction for the total work done in the movement of concrete through the hoppers. In contrast, FA spherical ball bearing particles could produce same total work done by minimizing waste work without SP dosage.

It is seen that, the compaction factor of 40 and 60 % FA mixes was reduced compared to the 20 % LS mix, while the slump of the 40 and 60 % FA mixes increased in the same comparison. Therefore, the determination of water retention capacity (WRC) of the fresh mixes will justify the workability (spread diameter) with/without free surface water, as given in Fig. 5 (e). The WRC of control sample was 0.63 and that of 20 % LS concrete was 0.65. It may be the retained water in the cenospheres of LS that could not be extracted at an applied vacuum pressure and the workability was slightly increased despite increased flaky and irregular shaped particles. However, the WRC of 40 and 60 % LS mixes was 0.57 and 0.50, respectively, and the WRC of 40–60 % LS samples was slightly reduced compared to the 20 % LS mix. Therefore, increased cenospheres, flaky, and irregular shaped particles for LS concretes proportionally reduced water retention capacity. Apart from LS as a SCM, the WRC of 20, 40, and 60 % FA samples was 0.58, 0.52, and 0.49, respectively. Therefore, the WRC of FA concretes was proportionally reduced with FA content. This may be due to the rounded FA particles that attributed loose particle packing among cement-FA-sand. Thus, the FA concretes provided higher inter-particle pore spacing, and the surface water of the mixes was rapidly extractable with same vacuum pressure compared to LS, and the mix lost flowability. As a result, the WRC of 60 % LS and FA concretes was reduced by 20.6 % and 22.2 % compared to the control mix, as shown in Fig. 5 (e).

Therefore, Fig. 5 provided a comprehensive characterisation of LS and FA concretes in plastic state viz. slump, air content, fresh density, compaction factor, and WRC. The fresh LS and FA concretes with/without SP provided design slump and air content for the mix design. The LS and FA concretes also provided normal density concrete and compatibility. In essence, 20–60 % LS showed similar fresh properties of concrete using 20–60 % FA as a SCM.

3.2. Mechanical properties

3.2.1. Compressive strength

The variation of the compressive strengths of LS and FA concretes at 7, 28, and 90 days are shown in Fig. 6 (a). Among all LS concretes, the 40 % LS yielded maximum compressive strength of 40.5 and 58.6 MPa, respectively at 7 and 90 days, while 20 % LS showed the maximum 28 days compressive strength of 49.3 MPa. For the FA concretes, the 20 % FA gained the maximum compressive strength of 34.5, 38.8, and 45 MPa at 7, 28, and 90 days, respectively. It is seen that, the minimum compressive strength was achieved by 60 % LS and 60 % FA mixes, at all test durations.

In this study, the 7, 28, and 90 days compressive strength of the control specimen was 40.5, 44.8, and 49.6 MPa, respectively. Based on the comparison of LS and FA concretes, the 40 % LS and 20 % FA mixes gained the maximum SAI of 100 % and 85 %, respectively at 7 days, while the minimum SAI was 45 % and 32 % for 60 % cement replacement by LS and FA, respectively. It is seen that 20–40 % LS as a partial replacement of cement accelerated the early age pozzolanic activity of the system compared to other mixes. The LS possess 31.6 % amorphous aluminosilicate phase, and the pozzolanic activity of LS initiates in between 3 and 7 days, and proportionally increases with the hydration duration [6]. The formation of Na, Mg, and K incorporated calcium aluminosilicate hydrate (C-A-S-H) amorphous intermediate hydration products provided nucleation sites in the crystalline phases of ettringite (AFt), secondary ettringite (AFm), and calcium silicate hydrate (C–S–H), and accelerated early age strength development of 20–40 % LS concrete mixes [6]. As a consequence, the SAI development of 20–40 % LS mixes was consistent at 28 and 90 days, and the maximum SAI was 118 % for 40 % LS mix at 90 days. In addition, the pH of LS was 11.28 and found less than the pH of FA, which is 12.17. However, the EC of FA was found to be 330 μS/cm, while that of LS was 1300 μS/cm. In essence, the reduced ion dissolution capacity of FA at higher alkalinity could not accelerate the strength development of FA concrete mixes, and hence FA is characterised as slow pozzolanic compared to LS in the same comparison. On the other hand, the 7, 28, and 90 days SAI of 20–40 % FA mixes were less compared to 20–40 % LS mixes. Specifically, the 7 days SAI of 20 % FA and 40 % FA mixes were 85 % and 32 %, respectively, whereas 90 days SAI were 91 %, and 53 %, respectively. A study mentioned the amorphousness of FA originating from same source was 54.6 % [33], but the grains are round with visible cenospheres (as shown in Fig. 3 (c)), and therefore the concrete prepared with 20–40 % FA left with high amount of pores leading to decrease in the early and long-term compressive strength development. In this study, the minimum recorded 90 days SAI was 90 % and 53 % for 60 % LS and 60 % FA mixes, respectively. The reduced ion dissolution capacity of FA along with the reduced alkalinity due to the clinker dilution highly reduced the compressive strength development of 60 % FA mix compared to 60 % LS mix [3,6,19].

The strength activity index (SAI) of 20–60 % LS and FA concretes were compared with the 75 % SAI requirements set by the standards BS 8615 [51], ASTM C618 [52], and AS 3582.4 [53] at 28 days, while RILEM TC 267-TRM [54] categorised concrete to be highly pozzolanic, moderately pozzolanic, and not pozzolanic when the SAIs within >100 %, 65–100 %, and <65 %. It is seen that 20–60 % LS and 20 % FA as a partial replacement of cement produced SAI >75 % and satisfy the requirement set by the standards BS 8615 [51], ASTM C618 [52], and AS 3582.4 [53] at 28 days. On the other hand, according to RILEM TC 267-TRM [54], 20–40 % LS are classified as a highly pozzolanic, and 60 % LS and 20–40 % FA are classified as moderately pozzolanic, and 60 % FA as non-pozzolanic.

3.2.2. Split tensile strength

The split tensile strength and relative split tensile strength of 0–60 %

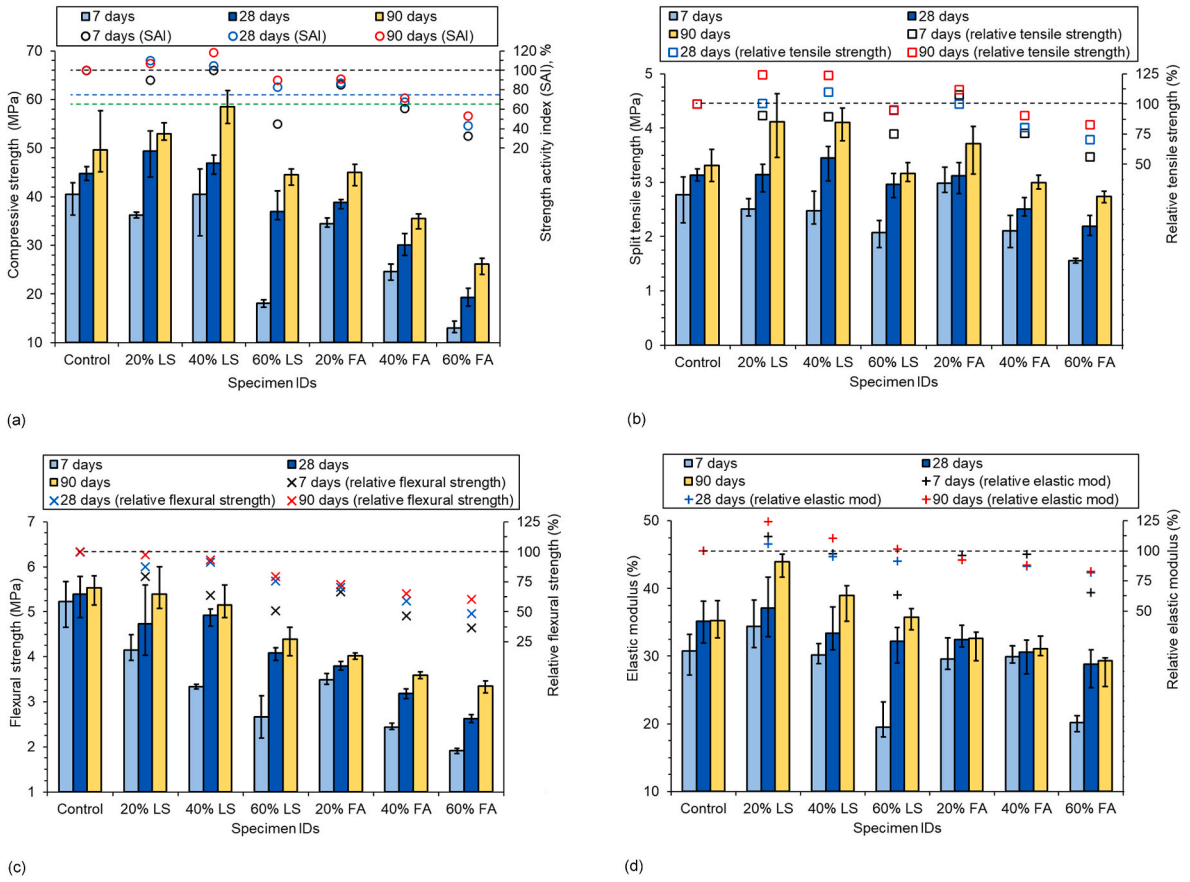

Fig. 6. Variation of the compressive strength and strength activity index (SAI) (a), split tensile strength and relative split tensile strength (b), flexural strength and relative flexural strength (c), and (d) elastic modulus and relative elastic modulus of control, 20–60 % LS, and 20–60 % FA concrete specimens. The error bars representing the maximum and minimum measured values. The blue dash line in Fig. 6 (a) represents the 75 % SAI requirements for BS 8615 [51], ASTM C618 [52], and AS 3582.4 [53] at 28 days, and green dash line at 65 % SAI points out the requirements of RILEM TC 267-TRM [54], respectively. The black dash line in Fig. 6 (a–d) indicates the mechanical property of the control specimen. (For interpretation of the references to colour in this figure legend, the reader is referred to the Web version of this article.)

cement replaced LS and FA concrete mixes is depicted in Fig. 6 (b). The LS and FA concretes produced a consistent split tensile strength development at 7, 28, and 90 days. The maximum split tensile strength was 4.11 MPa and 3.71 MPa for 20 % LS and 20 % FA mixes at 90 days, while the minimum tensile strength was 3.16 MPa and 2.74 MPa for 60 % LS and 60 % FA mixes in the same comparison. The 7, 28, and 90 days split tensile strengths of the control specimen were 2.77, 3.13, and 3.32 MPa, respectively. The 7 days maximum relative split tensile strength was 91 % and 108 % for 20 % LS and 20 % FA mixes, while the minimum value was 89 % and 56 % for 60 % LS and 60 % FA mixes. It is seen that the 20 % FA mix slightly induced the early age split tensile strength compared to the control and 20 % LS mixes. Later, the maximum 28 days relative spilt tensile strength was 110 % and 100 % for 40 % LS and 20 % FA concrete mixes, and in comparison, the minimum value was 95 % and 70 % for 60 % LS and 60 % FA mixes. The tensile strength development of 20–40 % LS mixes from 7 to 28 days was higher due to the increased ion dissolution capacity of the LS than FA. Here, the relative split tensile strength of 60 % FA mixes was increased by 14 % from 7 to 28 days and the increase in the development of tensile strength was found maximum compared to the 20–40 % FA mixes. This may be due to the high alkaline medium provided induced pozzolanic activity of 60 % FA mix in the formation of hydration products [55]. The maximum 90 days relative split tensile strength was 124 % and 112 % for both 20 % LS and 40 % LS, and 20 % FA mixes. Nonetheless, the minimum value was 95 % and 83 % for 60 % LS and 60 % FA mixes in the same comparison. Therefore, the ion dissolution potential of LS at reduced alkalinity consistently maintained the pozzolanic activity in the development of split tensile strength of LS concretes. However, high alkaline medium with lower ion dissolution potential of FA reduced the pozzolanic activity and split tensile strength of 40–60 % FA concrete mixes.

3.2.3. *Flexural strength*

The variation of the flexural strength of the 20–60 % LS and 20–60 % FA concrete mixes at 7, 28, and 90 days is shown in Fig. 6 (c). The LS and FA concrete mixes showed a consistent strength development over the testing period. The average maximum flexural strength of the control specimen was 5.23, 5.40, and 5.53 MPa at 7, 28, and 90 days. Among LS and FA mixes, the average maximum flexural strength was 5.40 and 5.15 MPa for 20 % LS and 20 % FA mixes at 90 days, respectively, while the average minimum flexural strength was 4.38 and 3.35 MPa for 60 % LS and 60 % FA mixes, respectively. The maximum relative 7 days flexural strength of 20 % LS and 20 % FA mixes was 79 % and 67 %, respectively, and the minimum was 51 % and 37 % for 60 % LS and 60 % FA mixes, respectively in the same comparison. At 28 and 90 days, the relative flexural strength of the same mixes were increased proportionally and produced the maximum and minimum relative flexural strength. It is seen that the incorporation of LS and FA as a SCM significantly reduced the relative flexural strength of the concrete mixes. The reduction of the flexural strength is more prominent at high cement replacement by the pozzolan that dilutes the clinker C_3S and β-C_2S phases [56]. In this study, 60 % LS mix induced 25 % relative flexural strength from 7 to 28 days while only 3 % from 28 to 90 days. A high volume of LS in the mix imparted higher early age ion dissolution that accelerated the formation of hydration products by combining available

clinker in the system and increased relative strength development from 7 to 28 days. In general, the ion dissolution capacity of pozzolans reduced at long term hydration and at 60 % cement replacement by LS, it is unlikely that any remaining clinker would be reacted due to the lower cement content in the system.

3.2.4. Elastic modulus

The variation of the elastic modulus of the control, 20–60 % LS, and 20–60 % FA concrete mixes is shown in Fig. 6 (d). In this study, a consistent development of the elastic modulus of LS and FA concrete mixes is depicted at 7, 28, and 90 days, but the elastic modulus of the concrete mixes degraded with the increase of SCM content. At 90 days, the maximum elastic modulus was 43.92 and 32.62 GPa for 20 % LS and 20 % FA concrete mixes, respectively. However, the 60 % LS and 60 % FA concrete mixes produced the minimum elastic modulus of 35.73 and 29.29 GPa at 90 days, respectively. The elastic modulus of the control specimen was 30.78, 35.12, and 35.27 GPa 7, 28, and 90 days, respectively. The relative maximum elastic modulus was 112 % and 97 % for 20 % LS and 40 % FA mixes, respectively at 7 days, while the minimum was 19.52 and 20.17 GPa for 60 % LS and 60 % FA mixes in the same comparison. At 28 and 90 days, the maximum relative elastic modulus was obtained for 20 % LS and 20 % FA mixes, while the minimum relative elastic modulus was yielded for 60 % LS and 60 % FA mixes. It is seen that alkalinity and ion dissolubility of 60 % LS and 60 % FA concrete mixes helped gaining 29 % and 16 % higher relative elastic modulus at 28 days compared to 7 days. Nonetheless, the relative compressive strength of 40 % LS was 10 % and 11 % higher compared to 20 % LS mix at 7 and 90 days, however, the relative elastic modulus of 40 % LS was decreased by 14 and 15 % at same comparison. The reduction of the elastic modulus of 40 % LS concrete mix may be due to the interfacial transition zone (ITZ) pores/air voids that could not be refined from early to extended lime curing [57,58]. Therefore, the increasing LS content as a SCM proportionally increased the elastic strain of the composite and making 40 % LS concrete more ductile despite high compressive elastic loading.

It can be seen that the physiochemical, microstructural, and electrical conductivity of LS provided strong justification in the characterisation of the fresh and mechanical properties of LS concretes compared to FA concretes. The mechanical strength development of LS concrete mixes can be interpreted through ITZ microstructure development and hydration products. Therefore, this study assessed the microstructure and hydration products development of 0–60 % LS concrete samples through SEM-EDS microscopy.

3.3. Microstructure

3.3.1. SEM

The SEM images of 0–60 % LS concrete mixes at 7 and 90 days are shown in Fig. 7. As LS is a new SCM and activates early in unsaturated lime solution than conventional FA, therefore this study will emphasis on the microstructure development of 0–60 % LS concrete mixes. Specifically, the mechanical strength development of 0–60 % LS mixes will depend upon the reactivity of LS in the development of the aggregate ITZ. The microstructure of 0–60 % LS concrete mixes provided characteristic change in the development of the aggregate ITZ from early age to long term strength growth. Particularly, the characteristic microstructural features include the microcracks and pores in the ITZ and non-ITZ zones, partially reacted and unreacted binders, and ettringite recrystallisation, which influences strength development of LS concretes [59]. In this study, partially hydrated cement (PHC), partially reacted LS (PRLS), and anhydrous LS (ALS) were identified from the layered EDS mapping of BSE images, and the characteristic variation is shown in Fig. 8 (a) and Fig. 8 (b) for control and 20 % LS mixes, respectively. The PHC, PRLS, and ALS were assessed from the grains with high

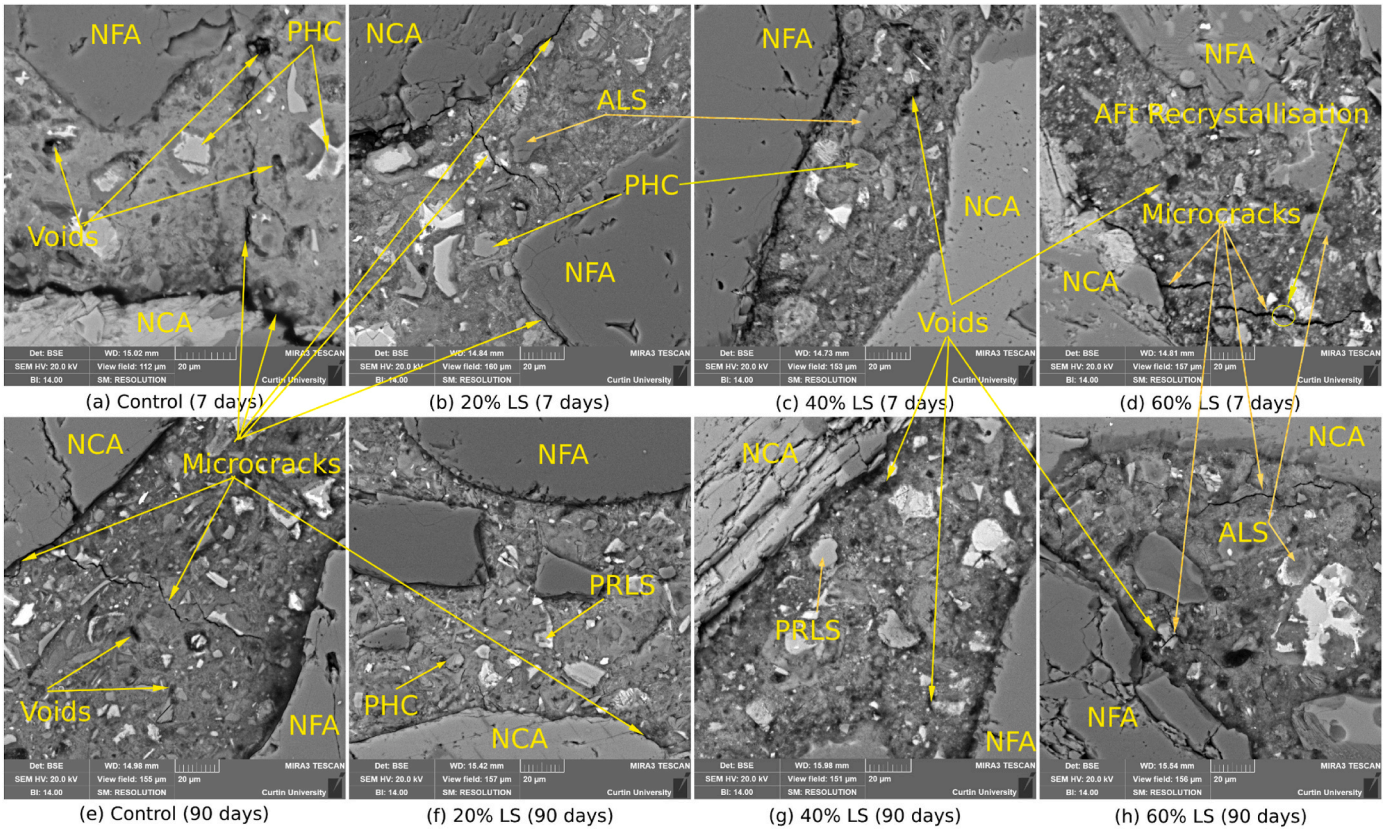

Fig. 7. BSE images of 0–60 % LS concrete mixes ITZ at 7 days (a–d), and 90 days (e–h). Here, PHC, PRLS, and ALS are partially hydrated cement, partially hydrated LS, and anhydrous LS.

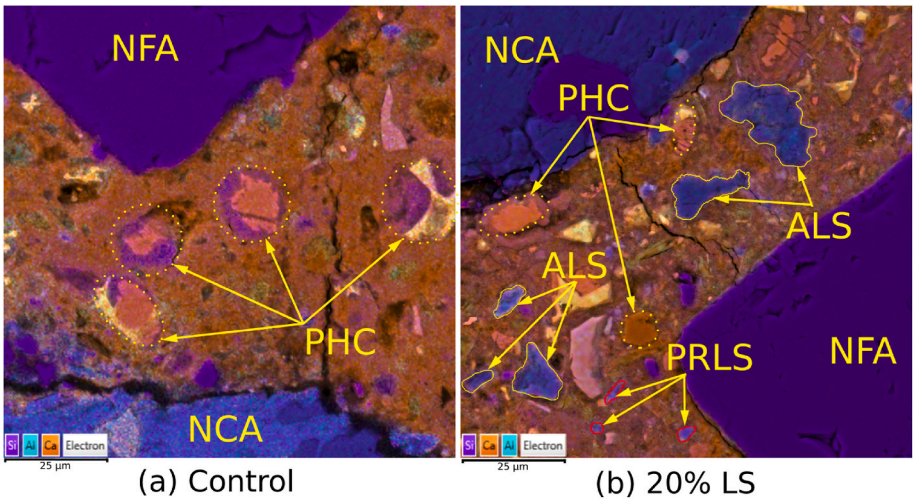

Fig. 8. Identification of PHC, PRLS, and ALS for control (a) and (b) 20 % LS from layered EDS mapping of BSE images of Fig. 7 (a) and (b).

concentration Ca at the core with peripheral Si, high concentration Si at core with circumferential Ca, and high concentration of Si and lower concentration of Al through appropriate colour identifications. Overall, microstructure of the concrete mixes was highly improved with the incorporation of LS as a SCM. At early age (7 days), the LS incorporated concrete mixes provided better ITZ compatibility than the control. It is seen that the control mix showed at least 1–3 μm visible gap in between the paste/mortar with the NCA ITZ, partially reacted cement grains in the matrix, non-ITZ microcracks, and voids, as shown in Fig. 7 (a). The NCA ITZ compatibility with paste/mortar slightly improved in the 20 % LS concrete, but microcracks of <1 μm width were still observed in the NCA ITZ (Fig. 7 (b)), and partially reacted cement and LS along with non-ITZ cracks and voids degraded the early age mechanical performance. In 40 % LS concrete as shown in Fig. 7 (c), the ITZ of NCA and NFA was improved to gain high early age compressive strength such that the cracks in the ITZ and partially reacted binder particles were minimised, but the system produced higher number of pores compared to 20 % LS mix. The 40 % LS mix diluted the cement clinker, but the mix gained higher early strength compared to 20 % LS, and this may be due to the higher early age ion dissolution capacity of LS that could combine available portlandite in the 40 % LS system making a highly compact microstructure left with minimum partially hydrated binders and microcracks. On the other hand, from Fig. 7 (d), the ITZ of 60 % LS mixes showed bridging microcracks of 1–2 μm width in the non-ITZ zones, left with higher amount of partially reacted and unreacted binders, and discrete pores. The white grains near the cracks indicated AFt recrystallisation, which provided expansion in the paste/mortar matrix to induce tensile microcracks in the 60 % LS mix. The ion dissolution of 60 % LS is higher compared to the other mixes. However, the reduced portlandite in the highly diluted cement system left with high amount of unreacted and partially reacted LS particles, which decreased the early age compressive strength of 60 % LS mix compared to other mixes.

At 90 days, the ITZ compatibility with paste/mortar of control concrete was highly improved with minimal microcracks and voids, but still higher amount of non-ITZ bridging cracks and partially hydrated and anhydrous cement particles were visible in the microstructure, as shown in Fig. 7 (e). For 20 % LS mix, the early age microcracks at the ITZ of NCA and NFA were reduced at long-term hydration. It is seen that early age large pores were healed, and anhydrous cement and LS grains were further hydrated making a dense microstructure (Fig. 7 (f)) to gain higher compressive strength at extended curing. The 40 % LS formed a highly dense microstructure (Fig. 7 (g)) at extended curing by consuming available portlandite and making highly compatible ITZ with mortar/paste with reduced pore sizes compared to the early age microstructure of the same mix. Lastly, the microcracks in the ITZ of NCA were highly reduced for 60 % LS at long-term curing (Fig. 7 (h)), however, the microcracks in the ITZ of NFA and non-ITZ regions are more pronounced. This may be due to the precipitation of highly reactive alkaline salts (Na, Mg, K) from the LS particles that incorporated in the C–S–H or C-A-S-H structure, which expanded the hydrated crystal structure and tensile stress exacerbates in the void-NFA-cement/mortar matrix to develop higher amount of microcracks [6,60,61]. Additionally, higher amount of anhydrous LS along, large pore voids at long-term hydration, and AFt recrystallisation through the bridging microcracks of paste/mortar in 60 % LS mix reduced the long-term mechanical strength in comparison to 0–40 % LS concrete mixes.

3.3.2. EDS

The line scan EDS were generated for the BSE images in Fig. 7(a–h) of 0–60 % LS mix samples and the elemental spectra of the ITZ in between the NCA and NFA are shown in Fig. 9. A cropped portion of the BSE image is attached in each elemental spectra in Fig. 9 where a line scan was generated. In general, the length of the ITZ of the NCA and NFA varies from 9 to 50 μm [60,62,63], and therefore, a 10 μm width box was placed near to the surface of NCA and NFA to identify the major concentrations (counts) of the elements in the formation of the probable hydration products. It can be seen significant concentration of S, Fe, Mg, and Al in the C–S–H in the ITZ of NFA which indicate the formation of AFt, AFm, M-A-S-H and C-A-S-H hydration products at 7 days, as shown in Fig. 9 (a) [6,64]. The line scan EDS in the ITZ of NCA indicated the formation of AFm, M-A-S-H, K-A-S-H, and C-A-S-H, as shown in Fig. 9 (a). Therefore, the formation of Mg and K based C–S–H along with AFt and AFm induced higher ITZ gap and microcracks in the NCA and NFA of the control specimen at 7 days [65]. At 90 days, the ITZ compatibility of NCA was highly improved but still Mg, K, and Al based C–S–H were formed, as shown in Fig. 9 (b), and the ITZ of NFA was concentrated with Al based C–S–H producing highly compatible ITZ. A high concentration of S and Al along with Ca and Si may form AFt, C-A-S-H, and C–S–H in the ITZ of NCA and NFA of 20 % LS sample at 7 days, as shown in Fig. 9 (c). The microcracks near the ITZ may be influenced by the formation of AFt and the mechanical strength was slightly reduced compared to the control at early age. Later, the hydration products in the ITZ of NFA incorporated K-A-S-H, and it may be the precipitated K from the lithium slag soluble salts that depleted Ca from C-A-S-H structure at long-term hydration [6,66], as shown in Fig. 9 (d). A similar elemental combination was found in the ITZ of NCA at both 7 and 90 days, however the ITZ microcracks were highly reduced at long-term hydration, as shown in Fig. 9 (d). For 40 % LS specimen, ITZ of NFA incorporated S, Fe, and Al with C–S–H that may form AFt, AFm, C-A-S-H, and C–S–H at 7 days, while the ITZ of NCA may contain AFt, K-A-S-H, C-A-S-H, and C–S–H, as

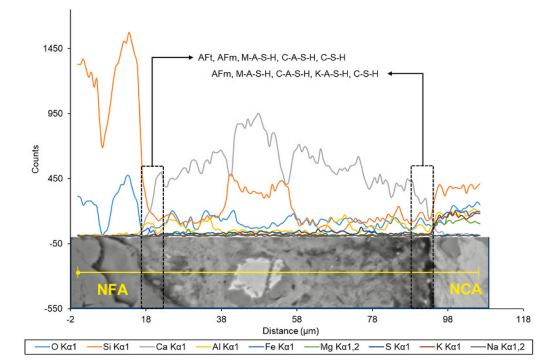

(a) Control (7 days)

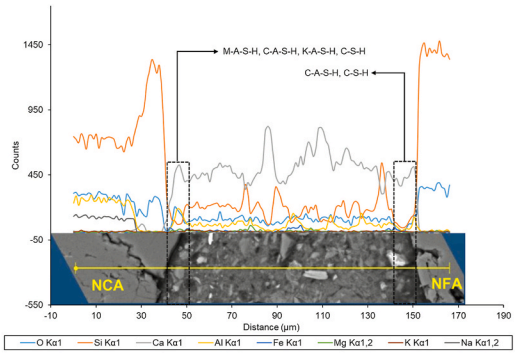

(b) Control (90 days)

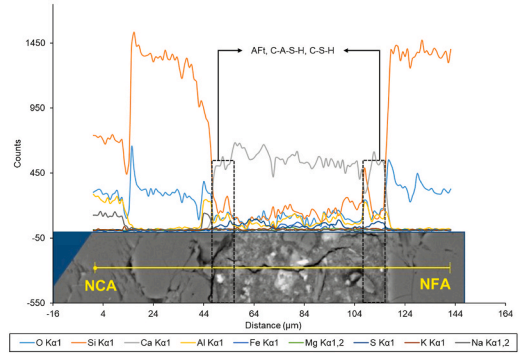

(c) 20% LS (7 Days)

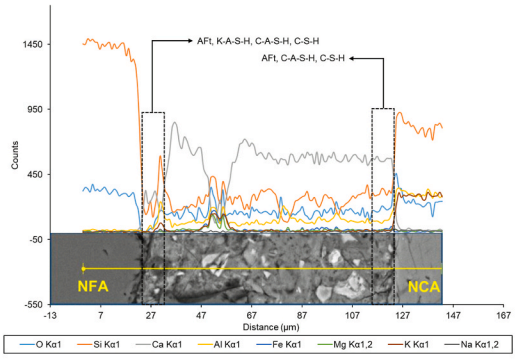

(d) 20% LS (90 Days)

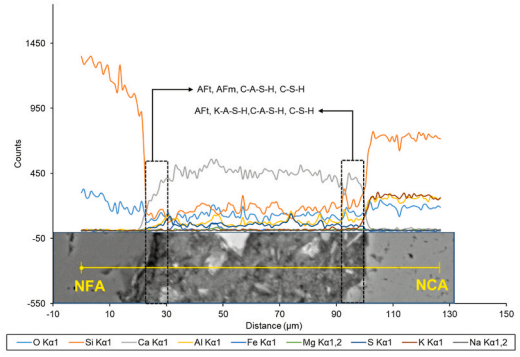

(e) 40% LS (7 Days)

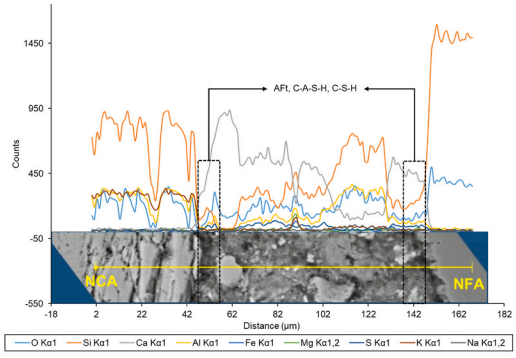

(f) 40% LS (90 days)

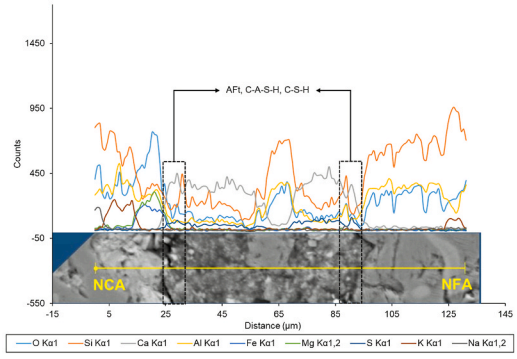

(g) 60% LS (7 days)

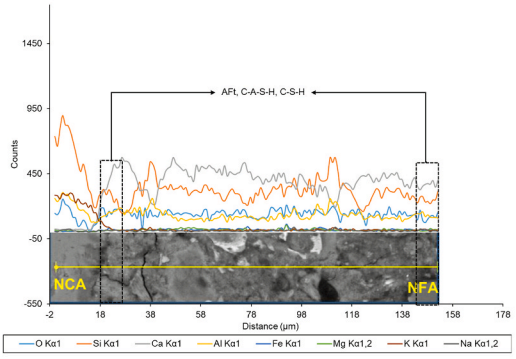

(h) 60% LS (90 days)

Fig. 9. Line scan EDS generated for the BSE images of 0–60 % LS concrete specimens of Fig. 7(a–h).

shown in Fig. 9 (e). It can be seen that ITZ of NFA showed a few hairline microcracks in 40 % LS sample and this may be due to the formation of AFt and AFm. In contrast, the NCA ITZ of 40 % LS comprised of AFt and K-A-S-H hydration products but did not indicate any visible microcracks at 7 days, and this may be due to working distance and preferred scaling of the BSE imaging that could not detail the fine microcracks in that region. At 90 days, the formation of AFt, C-A-S-H, and C–S–H indicated highly compatible ITZ for NCA and NFA of 40 % LS specimen, as shown in Fig. 9 (f). Therefore, the fine microcracks in the ITZ of 40 % LS specimen at early age were healed at 90 days to provide higher mechanical strength. Lastly, for 60 % LS specimen, the ITZ of NCA and NFA showed the formation of AFt, C-A-S-H, and C–S–H at 7 and 90 days, as shown in Fig. 9 (g) and (h), respectively. It is seen that the EDS signal for S was higher at 7 and 90 days compared to other elements under consideration. Therefore, the early age microcracks formed at the ITZ and non-ITZ zones of 60 % LS was associated with the formation of AFt, and the dilution of cement could not form new hydration products at long-term curing to improve the ITZ compatibility and in the development of mechanical strength.

The molar ratios of Al/Ca and Si/Ca of 0–60 % LS concrete mixes at 7 and 90 days are plotted in Fig. 10 to indicate the formation of crystalline, amorphous, and amorphous intermediate hydration products through kernel density estimation. In particular, least intermixed point method was adopted to fix the position of CH, AFt, AFm, and C-A-S-H in the Al/Ca versus Si/Ca plot [64,67,68]. At 7 days, the kernel density was highly concentrated near CH zone and partly dense at AFt and C-A-S-H, as shown in Fig. 10 (a), while the data density was shifted to C-A-S-H at 90 days, as depicted in Fig. 10 (e). It is seen that the data concentration of intermixed CH, AFt, and AFm with C-A-S-H were higher at 90 days than 7 days, and this may be the probable incorporation of Mg and K based A-S-H amorphous intermediate hydration products, as shown in Fig. 9 (a–b). Therefore, the formation of amorphous intermediate hydration products from the reorientation of C-A-S-H microstructure induced the long-term strength development of control specimen. For 20 % LS specimen, the kernel density was populated in between intermixed C-A-S-H and CH, C-A-S-H and AFt, and C-A-S-H at 7 days, respectively, as shown in Fig. 10 (b). The later age microstructure of 20 % LS specimen was highly improved and the data density of Al/Ca v/s Si/Ca was highly concentrated at C-A-S-H (in Fig. 10 (f)), while data density was highly reduced the intermixed C-A-S-H with CH, AFt, and AFm zones. On the other hand, data density of 40 % LS specimen were concentrated at C-A-S-H zone at early age, as shown in Fig. 10 (c), and as a result the specimen gained maximum SAI of 100 %. From Fig. 10 (g), the data density of 40 % LS at 90 days was expanded higher compared to 7 days, but still higher amount of retained intermixed C-A-S-H with AFt and AFm porous hydrated phases compared to 20 % LS (in Fig. 10 (f)). Lastly, the data density of 60 % LS specimen was higher in the border line of intermixed C-A-S-H with AFt and AFm phases at 7 days, as shown in Fig. 10 (d). Therefore, the early age SAI of 60 % LS was minimum at 83 %, and at 90 days, the maximum data density of Al/Ca v/s Si/Ca shifted to C-A-S-H. In addition, the data density of 60 % LS was highly shifted away from the intermixed C-A-S-H with AFt and AFm phases at longer hydration (in Fig. 10 (h)) compared to 20–40 % LS mixes, and this indicated the higher concentration of porous amorphous intermediate hydration products. It is seen that a small data density was continuing to enlarge near CH of 20–60 % LS specimen. This may be the residual CH that can still form hydration products at an extended duration of hydration.

4. Additional discussion

In this study, the compressive strength, tensile strength, flexural strength, and elastic modulus of LS and FA concretes will be estimated from the prediction equations proposed in different studies and standards. The proposed equations were verified for a wide range of pozzolans in different mix designs to understand the pozzolan reactivity at early and long-term hydration, and the modification required to characterise new pozzolans or conventional pozzolans with different sources, treatment, or test conditions etc. In this study, the strength prediction equations found in the standards and literature will be used to estimate the mechanical strength of LS and FA concretes. The compressive strength of control and fly ash concretes can be predicted from the Bolomey equation [69], as shown in Eq. (1), where $f_c(t)$, $A(t)$, C, W, and $B(t)$ represent compressive strength (MPa) at time t (in days), age function, cement content (kg/m^3), water content (kg/m^3), and a constant, respectively.

$$f_c(t) = A(t)\left(\frac{C}{W}\right) + B(t) \tag{1}$$

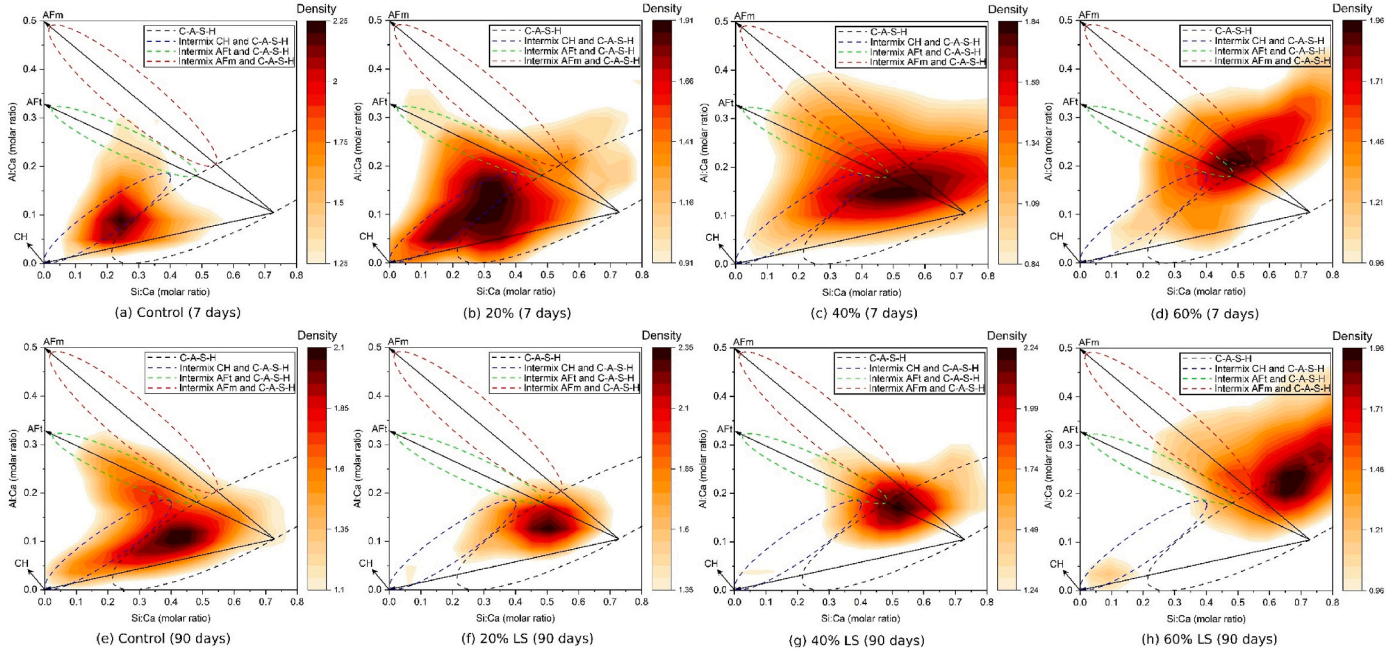

Fig. 10. Al/Ca (molar ratio) versus Si/Ca (molar ratio) through line scan EDS of 0–60 % LS concrete mixes at 7 and 90 days.

Here, the value of $A(t)$ was 30.1, 35, 39.2, and 41.2 at 7, 28, 180, and 365 days, respectively, while that of $B(t)$ was constant i.e., −18.2. Here, Eq. (1) was slightly modified to Eq. (2), where the reactivity of FA at different test durations were considered [69]. Here, a and b are regression constants of value 0.049 and 0.0255, respectively. Then, α_1, α_2, and P are pozzolanic activity factors for the contribution of compressive strength at different test ages, Blaine specific surface area function, and pozzolan content in the mix (kg/m^3).

$$f_c(t) = \left(\frac{t}{a+bt}\right)\left(\frac{\alpha_1\alpha_2 P + C}{W}\right) + B(t) \tag{2}$$

$$\alpha_1 = k_1(t)\exp\left\{k_2(t).\left(\frac{FA}{C}\right)\right\} \tag{3}$$

$$k_1(t) = m_1\{1 - \exp(-m_2 t) + m_3\} \tag{4}$$

$$k_2(t) = n_1\{1 - \exp(-n_2 t) + n_3\} \tag{5}$$

$$\alpha_2 = k_3(B - 250) + 1 \tag{6}$$

The parameters $k_1(t)$ and $k_2(t)$ are expressed as increasing functions of t. Specifically, $k_1(t)$ participate in the development of α_1 as the pozzolanic activity increases the strength with ages, while $k_2(t)$ decreases with age as the residual $Ca(OH)_2$ in the system decreases with the time. The term $k_1(t)$ was determined from the constants m_1, m_2, and m_3, and the values are 1.55, 0.0075, and 0.156, respectively, while the constant values of n_1, n_2, and n_3 are −0.075, 0.01, and −0.371, respectively to express $k_2(t)$. Finally, the α_2 was expressed by the constant k_3 of value 1.14×10^{-4} and B representing the Blaine specific surface area of the pozzolan. The recommended constant values were considered to predict compressive strengths at different ages and plotted with respect to the measured compressive strength, as shown in Fig. 11 (a). It can be seen that the calculated compressive strength was overestimated for FA concrete mixes and underestimated for LS concrete mixers. The regression coefficient (R^2) of the predicted and measured compressive strength of FA and LS concrete specimens was 0.95 and 0.45, respectively. The proposed Eq. (2) [69] was based on the pozzolanic activity of the FA with portlandite. Specifically, the model assumed that the ion dissolution capacity of FA reduces with age and the reactivity of FA in the portlandite system also decreases with age, as shown in Fig. 2. Therefore, the predicted compressive strength of the FA concrete was higher compared to the measured strength. In contrast, the ion dissolution capacity of LS was higher compared to the FA in both DI water and portlandite medium, and as a result the measured strength of LS concrete was higher compared to FA concrete specimens. In addition, the theoretical and relative conductivity of LS to attain the reaction equilibrium was faster compared to the FA, and therefore the α_1 and α_2 of Eq. (2) need further adjustment to improve the R^2 for measured versus predicted compressive strength of LS concrete. The variables of α_1 and α_2 are recalculated from the non-linear generalized reduced gradient method by minimizing the difference between the sum of squares of the calculated and measured compressive strength. The predicted values of m_1, m_2, m_3, n_1, n_2, n_3, and k_3 were 0.218, 15.931, 0.215, 0, 0.01, 0.787, and 2.84 × 10^{-3}, respectively, and the R^2 for the measured and calculated compressive strength becomes 0.90, as shown in Fig. 11 (a). On the other hand, the 28 days split tensile strength (f_{ct}) of LS and FA concretes was predicted from the AS 3600 [26], ACI 318 [25], and CEB-FIP 1990 [27] standard equations, as shown in Eqs. (7), (9) and (13), respectively.

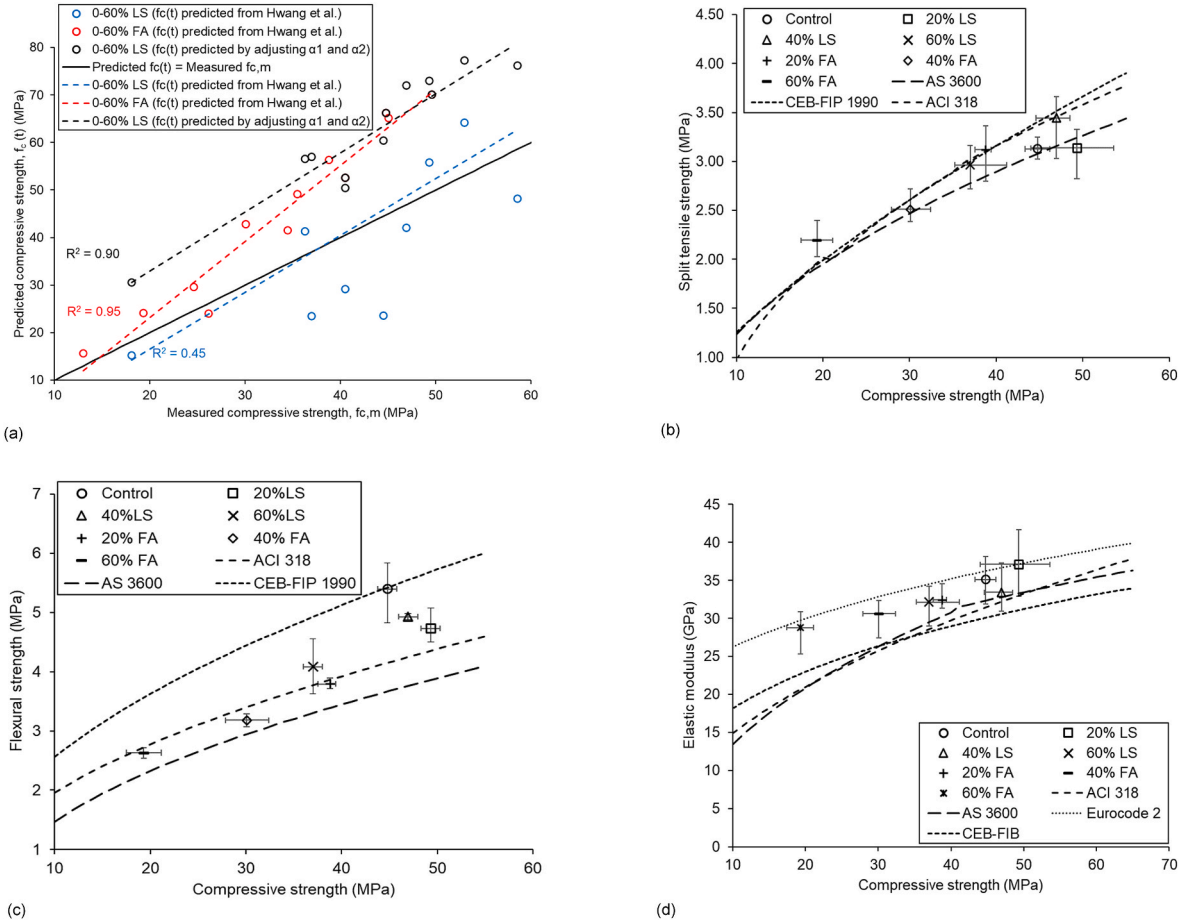

Fig. 11. Comparison of experimental and predicted compressive strength (a), tensile strength (b), flexural strength (c), and (d) elastic modulus of LS and FA concrete mixes. The horizontal error bars represent the maximum and minimum compressive strength.

$$f_{ct} = 0.36\sqrt{f_c^{'}} \quad (7)$$

$$f_{c,mi} = f_c^{'} + 3 \quad (8)$$

$$f_{ct} = 0.56\sqrt{f_c^{'}} \quad (9)$$

$$f_{c,m} = f_c^{'} + 7, f_c^{'} < 21\ MPa \quad (10)$$

$$f_{c,m} = f_c^{'} + 8.3, 21 < f_c^{'} \leq 35\ MPa \quad (11)$$

$$f_{c,m} = 1.1 f_c^{'} + 5, f_c^{'} > 35\ MPa \quad (12)$$

$$f_{ct} = 1.40\left(\frac{f_c^{'}}{10}\right)^{\frac{2}{3}} \quad (13)$$

Here, $f_c^{'}$, $f_{c,mi}$, and $f_{c,m}$ represent characteristic compressive strength of cylinder (MPa), mean in-situ compressive strength of the cylinder (MPa), and mean compressive strength of the cylinder (MPa). Eq. (8) was used for the determination of the f_c of Eq. (7), and Eqs. (10)–(12) were used to obtain $f_c^{'}$ of Eq. (9). The standard equations were used for the prediction of the split tensile strength of LS and FA concretes from the measured compressive strength are depicted in Fig. 11 (b). It is seen that CEB-FIP 1990 [27] underestimated the experimental split tensile strength of 20 % FA and 60 % FA mix specimens, and ACI 318 [25] underestimated the 20 % FA and 60 % FA concrete at 28 days. Nonetheless, AS 3600 only overestimated the split tensile strength of 20 % LS concrete mix. Therefore, AS 3600 [26] was found to be conservative in the prediction of the split tensile strength of LS and FA concrete mixes compared to ACI 318 [25] and CEB-FIP 1990 [27] standard equations. Later, the flexural strength ($f_{ct,f}$) of the LS and FA concrete mixes was predicted from the standard equations proposed by AS 3600 [26], ACI 318 [25], and CEB-FIP 1990 [27], as shown in Eqs. (14), (16) and (17), respectively.

$$f_{ct,f} = 0.36\sqrt{f_c^{'}} \quad (14)$$

$$f_{ct,m} = 1.4 f_{ct,f} \quad (15)$$

$$f_{ct,f} = 0.62\sqrt{f_c^{'}} \quad (16)$$

$$f_{ct,f} = 0.81\sqrt{f_c^{'}} \quad (17)$$

Where, $f_{ct,m}$ is the mean flexural strength. The predicted flexural strength of the LS and FA concrete mixes from the 28 days compressive strength is shown in Fig. 11 (c). It is seen that CEB-FIP 1990 [27] model overestimated the 28 days flexural strength of all mixes, while AS 3600 [26] underestimated the flexural strength of all mixes in the same comparison. In addition, ACI 318 [25] overestimated the flexural strength of 20–60 % LS mixes. Therefore, ACI 318 [25] and AS 3600 [26] was found to be conservative in the prediction of the flexural strength of the 0–60 % LS mixes from the measured compressive strength of the cylinders. Furthermore, the elastic modulus (E_c) of the LS and FA concrete mixes was predicted from the measured 28 days compressive strength of the cylinder by using the ACI 318 [25], AS 3600 [26], Eurocode 2 [70], and CEB-FIP 1990 [27], as shown in Eqs. (18) and (19) (a, b), 20, and 21, respectively.

$$E_c = 4700\sqrt{f_c^{'}} \quad (18)$$

$$E_c = \left(\rho^{1.5}\right) \times \left(0.043 f_{c,mi}^{0.50}\right), f_{c,mi} \leq 40\ MPa \quad (19a)$$

$$E_c = \left(\rho^{1.5}\right) \times \left(0.024 f_{c,mi}^{0.50} + 0.12\right), f_{c,mi} > 40\ MPa \quad (19b)$$

$$E_c = 22000 \times \left(\frac{f_{c,m}}{10}\right)^{0.3} \quad (20)$$

$$f_{c,m} = f_c^{'} + 8 \quad (21)$$

$$E_c = 0.85 \times 21500 \times \left(\frac{f_c^{'}}{10}\right)^{\frac{2}{3}} \quad (22)$$

Here, ρ represents the dry density of the concrete specimen. The measured 28 days compressive strength was used for the prediction of the elastic modulus of the LS and FA concrete specimens, as shown in Fig. 11 (d). It is seen that ACI 318, CEB-FIP 1990, and AS 3600 underestimated the elastic modulus of the concrete mixes, while Eurocode 2 marginally overestimated 20 % LS concrete mix elastic modulus. Therefore, the prediction of the elastic modulus from the standards ACI 318, CEB-FIP 1990, and AS 3600 was found to be conservative compared to Eurocode 2 in the prediction of the 0–60 % LS concrete mixes. In essence, the prediction compressive strength, split tensile strength, flexural strength, and elastic modulus from the literature and standardised equations provided the justification of the mechanical strength development of the 20–60 % LS concrete mixes as a normal concrete mix in line 20–60 % FA concrete mixes.

5. Conclusions

This study presents the fresh, mechanical, and microstructural properties of concretes containing various lithium slag (LS) contents of 20, 40 and 60 % and benchmarked with corresponding class F fly ash (FA) concretes and control ordinary Portland cement concrete. Based on above discussion, the following conclusions can be drawn.

a. The SiO_2+Al_2O_3+Fe_2O_3, loss of ignition at 750 °C, and amorphousness of raw-LS were 77.2 %, 7.8 %, and 31.6 %, respectively. The electrical conductivity and pH of the raw-LS were 1300 μS/cm and 11.28, respectively. The ion dissolution and CaO removal capacity tests of the pozzolan showed that LS was activated 11.6 days earlier than FA. These measured physio-chemical properties raw-LS are comparable with conventional FA properties. Therefore, 20–60 % LS was used as a partial replacement of cement for determination of fresh, mechanical, and microstructural properties of concrete.
b. The slump, air content, fresh density, and compaction factor of 20–60 % LS concrete were within 125 ± 25 mm, 2 ± 0.5 %, 2200–2600 kg/m^3, and 0.984 ± 0.004, respectively. These measured values were within the range of normal concrete fresh parameters. The water retention capacity of 20–60 % LS concrete was higher compared to FA concrete at same cement replacement. Therefore, the pore spaces in FA fresh concretes were higher than LS concrete at same cement replacement.
c. The compressive strength, tensile strength, and flexural strength of 40 % LS concrete were 46.9 MPa, 3.44 MPa, and 4.93 MPa, respectively at 28 days, and found higher compared to the control mix; replacing more than 40 % cement by LS highly reduced the mechanical strength properties. The strength activity index (SAI) of 40 % LS concrete was 118 % at 90 days, and the SAI is dropped by 28 % at 60 % LS content. The tensile strength, flexural strength, and elastic modulus of 20–60 % LS concrete was higher at all test ages compared to FA concrete at same replacement level.
d. The interfacial transition zone (ITZ) of 40 % LS concrete was free from microcracks at 7 and 90 days, but still contains large number of pores and partially hydrated and anhydrous LS.
e. It is seen that the amorphous C-A-S-H, and amorphous intermediate intermixed C-A-S-H with AFt and AFm hydration products increased with the increasing volume of LS, providing high mechanical strength but with large number of pores at long-term hydration.

f. The prediction of the compressive strength of LS concrete based on the equation proposed by Hwang et al. [69] for the strength development of FA concrete produced poor regression coefficient (R^2) of 0.45. The factors controlling the pozzolanic activity to induce strength with ages and Blaine specific surface area were adjusted by implementing a non-linear generalized reduced gradient method, and the R^2 for the same data set reached at 0.90. Also, AS 3600 [26] and ACI 318 [25] underestimated 28 days tensile strength, flexural strength, and elastic modulus of 40 % LS concrete. In contrast, the CEB-FIP 1990 [27] overestimated tensile and flexural strengths of 40 % LS concrete, and the Eurocode 2 [70] overestimated the elastic modulus in the same comparison.

The hydration products of amorphous intermediate intermixed C-A-S-H with AFt and AFm phases increases with the increase of LS content as a SCM. This amorphous intermediate phases also incorporates highly reactive alkali metal ions of K, Mg, and Na at later age. These precipitated ions may incorporate in C-A-S-H crystal structure and radiate tensile cracks in the ITZ/non-ITZ zones, making the microstructure porous. Therefore, in-depth durability assessment should be carried out for a convenient implementation of LS in concrete.

CRediT authorship contribution statement

SM Arifur Rahman: Data curation, Investigation, Methodology, Writing – original draft. **Faiz Uddin Ahmed Shaikh:** Conceptualization, Funding acquisition, Resources, Supervision, Writing – review & editing. **Prabir Kumar Sarker:** Conceptualization, Supervision, Writing – review & editing.

Declaration of competing interest

The authors declare that they have no known competing financial interests or personal relationships that could have appeared to influence the work reported in this paper.

Data availability

No data was used for the research described in the article.

Acknowledgements

This research was financially supported by the Australian Research Council (ARC) discovery project DP200102784. The authors are grateful to Jason Elliott and Vick Subra of Cementaid International Limited for their contribution of 20 L superplasticizer for the research support.

References

[1] S.A. Rahman, F.U.A. Shaikh, P.K. Sarker, A comprehensive review of properties of concrete containing lithium refinery residue as partial replacement of cement, Construct. Build. Mater. 328 (2022) 127053.
[2] S. Khair, et al., Evaluating lithium slag for geopolymer concrete: a review of its properties and sustainable construction applications, Case Stud. Constr. Mater. 20 (2024) e02822.
[3] E. Villar-Cociña, et al., Kinetics of the pozzolanic reaction between lime and sugar cane straw ash by electrical conductivity measurement: a kinetic–diffusive model, Cement Concr. Res. 33 (4) (2003) 517–524.
[4] J. Fan, et al., Heavy metals immobilization of ternary geopolymer based on nickel slag, lithium slag and metakaolin, J. Hazard Mater. 453 (2023) 131380.
[5] C. Li, et al., Preparation of lightweight ceramsite from solid waste lithium slag and fly ash, Construct. Build. Mater. 398 (2023) 132419.
[6] S.A. Rahman, et al., Assessment of lithium slag as a supplementary cementitious material: pozzolanic activity and microstructure development, Cement Concr. Compos. (2023) 105262.
[7] Z.-h. He, L.-y. Li, S.-g. Du, Mechanical properties, drying shrinkage, and creep of concrete containing lithium slag, Construct. Build. Mater. 147 (2017) 296–304.
[8] X. Luo, et al., Performance characterization and optimization of cement-lithium powder-grain slag composite cementitious materials, Construct. Build. Mater. 409 (2023) 133851.
[9] Y. Wang, et al., Thermal activation mechanism and activity evaluation of lithium slag: insights from simulated hydration, Construct. Build. Mater. 411 (2024) 134615.
[10] X. Gu, et al., Synergistic effect and mechanism of lithium slag on mechanical properties and microstructure of steel slag-cement system, Construct. Build. Mater. 396 (2023) 131768.
[11] S. Rahman, et al., Fresh state and hydration properties of high-volume lithium slag cement composites, Mater. Struct. 56 (4) (2023) 1–19.
[12] Y. Qin, et al., The mechanical properties of recycled coarse aggregate concrete with lithium slag, Adv. Mater. Sci. Eng. 2019 (2019) 1–12.
[13] GB 50010, Code for Design of Concrete Structures, Ministry of Housing and Urban-Rural Construction of the People's Republic of China and the General Administration of Quality Supervision, Inspection and Quarantine of the People's Republic of China: China, 2015.
[14] A. Zidol, M.T. Tognonvi, A. Tagnit-Hamou, Concrete incorporating glass powder in aggressive environments, ACI Mater. J. 118 (2) (2021).
[15] V. Venkitasamy, et al., Mechanical and durability properties of structural grade heavy weight concrete with fly ash and slag, Cement Concr. Compos. 145 (2024) 105362.
[16] G. Li, X. Zhao, Properties of concrete incorporating fly ash and ground granulated blast-furnace slag, Cement Concr. Compos. 25 (3) (2003) 293–299.
[17] H. Feng, et al., Development and design of ultra-high ductile magnesium phosphate cement-based composite using fly ash and silica fume, Cement Concr. Compos. 137 (2023) 104923.
[18] J. Yoon, et al., Characterization and quantification of the pozzolanic reactivity of natural and non-conventional pozzolans, Cement Concr. Compos. 133 (2022) 104708.
[19] S. Donatello, M. Tyrer, C.R. Cheeseman, Comparison of test methods to assess pozzolanic activity, Cement Concr. Compos. 32 (2) (2010) 121–127.
[20] I.R. Mocharla, et al., Performance and life-cycle assessment of high-volume fly ash concrete mixes containing steel slag sand, Construct. Build. Mater. 341 (2022) 127814.
[21] L. Jiang, V. Malhotra, Reduction in water demand of non-air-entrained concrete incorporating large volumes of fly ash, Cement Concr. Res. 30 (11) (2000) 1785–1789.
[22] American Coal Ash Association, Fly Ash Facts for Highway Engineers, US Department of Transportation, Federal Highway Administration, 2003.
[23] K.E. Seto, C.J. Churchill, D.K. Panesar, Influence of fly ash allocation approaches on the life cycle assessment of cement-based materials, J. Clean. Prod. 157 (2017) 65–75.
[24] D.K. Panesar, D. Kanraj, Y. Abualrous, Effect of transportation of fly ash: life cycle assessment and life cycle cost analysis of concrete, Cement Concr. Compos. 99 (2019) 214–224.
[25] ACI 318, Building Code Requirements for Structural Concrete and Commentary, Amarican Concrete Institute, Indianapolis, IN, USA, 2022.
[26] AS 3600, Concrete Structures - Commentary (Supplement 1 to AS 3600:2018). 2022, (Standards Australia: Australia).
[27] CEB-FIP, Model code 90, in Bulletin D'information. 1990, International Federation for Structural Concrete: Switzerland.
[28] G. Curran, Coal, climate and change: the narrative drivers of Australia's coal economy, Energy Res. Social Sci. 74 (2021) 101955.
[29] AS 3972, General Purpose and Blended Cements. 2010, (Standards Australia: Australia).
[30] ASTM C187, Standard Test Method for Amount of Water Required for Normal Consistency of Hydraulic Cement Paste, American Society for Testing Materials, USA, 2016.
[31] AS/NZS 2350.5, Methods of Testing Portland, Blended and Masonry Cements Method 5: Determination of Soundness, 2006. Standards Australia: Australia).
[32] AS/NZS 2350.4, Methods of Testing Portland, Blended and Masonry Cements, Method 4: Setting Time, 2006, pp. 1–8. Standards Australia/Standards New Zealand: Australia.
[33] A. Van Riessen, N. Chen-Tan, Beneficiation of Collie fly ash for synthesis of geopolymer Part 2–Geopolymers, Fuel 111 (2013) 829–835.
[34] N.W. Chen-Tan, Geopolymer from a Western Australian Fly Ash, Curtin University, 2010.
[35] J. Payá, et al., Enhanced conductivity measurement techniques for evaluation of fly ash pozzolanic activity, Cement Concr. Res. 31 (1) (2001) 41–49.
[36] G. Wei, et al., Deep insight into reactive chemical structures of Class F fly ash, Cement Concr. Compos. 142 (2023) 105195.
[37] Cementaid Superplastet F, Specification for Superplastet F, C.I. Ltd., 2016. Australia.
[38] AS 1379, Specification and Supply of Concrete, 2007, p. 56. Satandards Australia: Australia.
[39] AS 1012.5, Methods of Testing Concrete, Method 5: Determination of Mass Per Unit Volume of Freshly Mixed Concrete, 2014. Standards Australia: Australia.
[40] AS 1012.3.1, Methods of Testing Concrete, Method 3.1: Methods for the Determination of Properties Related to the Consistency of Concrete - Slump Test, 2014, p. 20. Standards Australia: Australia.
[41] AS 1012.4.2, Methods of Testing Concrete, Method 4.2: Determination of Air Content of Freshly Mixed Concrete - Measuring Reduction in Air Pressure in Chamber above Concrete, 2014. Standards Australia: Australia).
[42] AS 1012.4.1 Methods of testing concrete, Method 4.1: Determination of Air Content of Freshly Mixed Concrete - Measuring Reduction in Concrete Volume with Increased Air Pressure, 2014, p. 12. Standrads Australia: Australia.

[43] AS 1012.3.2, Methods of Testing Concrete, Method 3.2: Methods for the Determination of Properties Related to the Consistency of Concrete - Compacting Factor Test, 2014. Standards Australia: Australia).
[44] ASTM 1506, Standard Test Method for Water Retention of Hydraulic Cement-Based Mortars and Plasters, American Society for Testing Materials, USA, 2017.
[45] AS 1012.11, Methods of Testing Concrete, Method 11: Determination of the Modulus of Rupture, 2000. Standards Australia: Australia.
[46] AS 1012.17, Methods of Testing Concrete, Method 17: Determination of the Static Chord Modulus of Elasticity and Poisson's Ratio of Concrete Specimens, 1997, p. 16. Standards Australia: Australia.
[47] A. Hanif, Z. Lu, Z. Li, Utilization of fly ash cenosphere as lightweight filler in cement-based composites – a review, Construct. Build. Mater. 144 (2017) 373–384.
[48] S.K. Patel, et al., Durability and microstructural properties of lightweight concrete manufactured with fly ash cenosphere and sintered fly ash aggregate, Construct. Build. Mater. 226 (2019) 579–590.
[49] M.O. Mohsen, et al., Fly ash and natural pozzolana impacts on sustainable concrete permeability and mechanical properties, Buildings 13 (8) (2023) 1927.
[50] A.M. Neville, Properties of Concrete, vol. 4, Longman London, 1995.
[51] BS 8615-1, Specification for Pozzolanic Materials for Use with Portland Cement Natural Pozzolana and Natural Calcined Pozzolana, British standard, 2019.
[52] ASTM C618, Standard Specification for Coal Fly Ash and Raw or Calcined Natural Pozzolan for Use in Concrete, American Society for Testing Materials, USA, 2019.
[53] AS 3582.4, Supplementary Cementitious Materials, Part 4: Pozzolans — Manufactured (FOREIGN STANDARD), 2022. Standards Australia: Australia).
[54] D. Londono-Zuluaga, et al., Report of RILEM TC 267-TRM phase 3: validation of the R3 reactivity test across a wide range of materials, Mater. Struct. 55 (5) (2022) 142.
[55] C. Gu, et al., Study on early-age tensile properties of high volume fly ash concrete, Mater. Struct. 55 (5) (2022) 135.
[56] N. Abdelmelek, E. Lubloy, Flexural strength of silica fume, fly ash, and metakaolin of hardened cement paste after exposure to elevated temperatures, Journal of Thermal Analysis and Calorimetry 147 (13) (2022) 7159–7169.
[57] R. E, S. Hatanaka, Prediction of porosity of pervious concrete based on its dynamic elastic modulus, Results in Materials 10 (2021) 100192.
[58] G. Zhang, et al., Experimental and theoretical prediction model research on concrete elastic modulus influenced by aggregate gradation and porosity, Sustainability 13 (4) (2021) 1811.
[59] K.L. Scrivener, Backscattered electron imaging of cementitious microstructures: understanding and quantification, Cement Concr. Compos. 26 (8) (2004) 935–945.
[60] H. Wong, et al., Influence of the interfacial transition zone and microcracking on the diffusivity, permeability and sorptivity of cement-based materials after drying, Mag. Concr. Res. 61 (8) (2009) 571–589.
[61] K.L. Scrivener, A.K. Crumbie, P. Laugesen, The interfacial transition zone (ITZ) between cement paste and aggregate in concrete, Interface Sci. 12 (2004) 411–421.
[62] T. Akçaoğlu, M. Tokyay, T. Çelik, Effect of coarse aggregate size and matrix quality on ITZ and failure behavior of concrete under uniaxial compression, Cement Concr. Compos. 26 (6) (2004) 633–638.
[63] H. Zhao, et al., Numerical insights into the effect of ITZ and aggregate strength on concrete properties, Theor. Appl. Fract. Mech. 120 (2022) 103415.
[64] M. Chabannes, et al., Performance and microstructure development of lime–calcined fluvial sediment binders under different curing conditions, Cement Concr. Res. 160 (2022) 106903.
[65] S. He, et al., Distribution of porosity surrounding a microfiber in cement paste, Cement Concr. Compos. 142 (2023) 105188.
[66] P. Hemstad, et al., The effect of varying cement replacement level on alkali metal distribution in cement pastes, Cement Concr. Compos. 146 (2024) 105344.
[67] V. Hallet, et al., Hydration of blended cement with high volume iron-rich slag from non-ferrous metallurgy, Cement Concr. Res. 151 (2022) 106624.
[68] J.E. Rossen, K.L. Scrivener, Optimization of SEM-EDS to determine the C–A–S–H composition in matured cement paste samples, Mater. Char. 123 (2017) 294–306.
[69] K. Hwang, T. Noguchi, F. Tomosawa, Prediction model of compressive strength development of fly-ash concrete, Cement Concr. Res. 34 (12) (2004) 2269–2276.
[70] Eurocode 2, Eurocode 2: Design of Concrete Structures, 2004, p. 230. British Standard.